NASA TECHNICAL NOTE

NASA TN D-2761

NASA TN D-2761

AFTERBODY PRESSURES ON BOATTAILED BODIES OF REVOLUTION HAVING TURBULENT BOUNDARY LAYERS AT MACH 6

by W. Frank Staylor and Theodore J. Goldberg

Langley Research Center

Langley Station, Hampton, Va.

NATIONAL AERONAUTICS AND SPACE ADMINISTRATION • WASHINGTON, D. C. • MAY 1965

NASA TN D-2761

AFTERBODY PRESSURES ON BOATTAILED BODIES OF REVOLUTION HAVING TURBULENT BOUNDARY LAYERS AT MACH 6

By W. Frank Staylor and Theodore J. Goldberg

Langley Research Center
Langley Station, Hampton, Va.

NATIONAL AERONAUTICS AND SPACE ADMINISTRATION

For sale by the Clearinghouse for Federal Scientific and Technical Information
Springfield, Virginia 22151 – Price $2.00

AFTERBODY PRESSURES ON BOATTAILED BODIES OF REVOLUTION HAVING TURBULENT BOUNDARY LAYERS AT MACH 6

By W. Frank Staylor and Theodore J. Goldberg
Langley Research Center

SUMMARY

22605

An experimental investigation has been conducted to determine the effects of boattailing and angle of attack upon base and boattail pressures for bodies of revolution. Afterbodies with boattail angles from 0° to 24° at angles of attack up to 12° were tested at a free-stream Mach number of 5.98 and at a Reynolds number sufficient to cause a turbulent boundary layer to exist ahead of the afterbodies at zero angle of attack.

A simple method for predicting boattail pressures is presented, which gave a reasonable estimate for the present data. A correlation of existing base-pressure data was made for boattailed bodies of revolution with turbulent boundary layers and from this correlation base pressure as a function of boattail angle and cylinder Mach number can be estimated. Experimental data and the present calculations indicate that afterbody pressure drag can be substantially reduced with a relatively short boattail at Mach numbers from 1.5 to 6.0.

INTRODUCTION

Previous investigations have shown that afterbody drag constitutes a substantial part of the total drag on bodies of revolution at supersonic speeds (for example, see refs. 1 to 10). Chapman (ref. 1) has reported that in certain instances afterbody drag can amount to as much as two-thirds of the total body drag. At high supersonic speeds theoretical and experimental investigations have indicated that the afterbody continues to contribute a large part of the total drag for minimum drag bodies of revolution although the afterbody drag influence is somewhat lessened from that at low supersonic speeds.

The use of boattailing as a means of reducing afterbody drag has been studied rather thoroughly in the Mach number range from 1 to about 3. In many of these experimental investigations the effect of boattailing on base pressure was determined and the boattail surface pressures were estimated by theoretical means; whereas in a few other investigations (for example, refs. 10 to 13) both the boattail and base pressures were measured to obtain an experimental afterbody pressure drag. At Mach numbers greater than 3.5 very little base-pressure data exist for boattailed bodies of revolution and the present authors have no knowledge of any such data for boattail surface pressures. Since the projected

area of the boattail may be greater than the base area, the boattail drag can be a major part of the total afterbody drag. Therefore, emphasis should also be placed upon methods for predicting boattail pressures as well as base pressures in order to have the necessary parameters available to minimize afterbody drag.

The purpose of the present investigation was to obtain base and boattail pressures on bodies of revolution at hypersonic speeds and to correlate them with previous data at lower Mach numbers. This investigation was generally limited to turbulent boundary layers because previous studies have shown that Reynolds number has little effect on base pressure for bodies having turbulent boundary layers (refs. 1, 2, 3, 9, and 14) and because these bodies are representative of many full-scale hypersonic applications. Most of the tests were performed at a free-stream Reynolds number of 7.0×10^6 per foot in the Langley 20-inch Mach 6 tunnel. Nineteen model configurations were obtained by varying the nose section and afterbody and each configuration was tested at angles of attack up to 12°.

SYMBOLS

C_A component of axial-force coefficient due to afterbody drag based on model cross-sectional area

$C_{A,min}$ component of minimum axial-force coefficient due to afterbody drag based on model cross-sectional area

C_p pressure coefficient

ΔC_p error in pressure coefficient

D model cylinder diameter

d_s sting diameter

l_{bt} boattail axial length

l_s sting length

M Mach number

p static pressure

R Reynolds number based on model length

x axial distance referenced from a point one model diameter upstream of afterbody base

x' axial distance referenced from boattail-cylinder junction

y radial distance from center line

α angle of attack

β boattail angle

β_{min} boattail angle for minimum afterbody pressure drag

δ boundary-layer thickness

μ Mach angle, $\sin^{-1}\frac{1}{M}$

ν Prandtl-Meyer expansion angle

ϕ radial angle from windward stream line

Subscripts:

∞ free-stream condition

b base

bt boattail

c cylinder or flat plate immediately ahead of afterbody

p first peak pressure rise

APPARATUS AND TEST METHODS

Wind Tunnel

The present investigation was conducted in the Langley 20-inch Mach 6 tunnel which is an intermittent-type tunnel that exhausts through a movable second minimum to the atmosphere with the aid of an ejector. Stagnation pressure and temperature were approximately 400 psia and 450° F, respectively, for most of the tests; these tunnel conditions resulted in a Reynolds number per foot of 7.0×10^6. The stagnation conditions were varied for a few of the tests and a range of Reynolds number per foot from 3.3×10^6 to 10.0×10^6 was obtained. A more complete description of the tunnel is given in reference 15.

Model and Support

The basic model was a cylinder 10 inches in length and $3\frac{3}{8}$ inches in diameter with three nose sections and nine afterbody sections. (See fig. 1(a).) The three nose sections were a 15° (nose section 1) and a 45° (nose section 2) half-angle cone and a hemisphere (nose section 3) each of which had a radial

transition band on its surface to promote a turbulent boundary layer on the model. These bands consisted of 0.050-inch-diameter (average) grit that was bonded to the surface with a resinous substance. Eight afterbody sections were conically boattailed from 0° to 21° in 3° increments over an axial length of 1.18 inches ($l_{bt}/D = 0.35$) and one afterbody section consisted of a circular-arc (C.A.) boattail with a trailing-edge angle of 24°. Each of the afterbody sections was 4 inches long and had 12 pressure orifices on the cylinder and boattail surfaces and 4 pressure orifices on the base surface. (Coordinates of the orifices are listed in fig. 1(a)). The plane of the orifices was varied by rotating the model with respect to the sting, and the models were pivoted in the horizontal plane for angle of attack. The various configurations that were tested are listed in the following table:

Nose section	Boattail angle, β	Radial angle, ϕ
15° half-angle cone	0°, 3°, 6°, 9°, 12°, 15°, 18°, 21°, C.A.	0°, 45°, 90°, 135°, 180°
45° half-angle cone	0°, 6°, 12°, 18°, C.A.	0°, 180°
Hemisphere	0°, 6°, 12°, 18°, C.A.	0°, 180°

The 0° and 21° boattail afterbodies were tested with stings of 0.85, 1.15, 1.25, 1.50, 1.75, and 1.94 inches in diameter and 10.03 inches in length; the 1.25-inch-diameter sting had a sliding collar to simulate sting length. Also, a $4\frac{1}{16}$-inch-diameter disk could be attached directly behind the 0° boattail afterbody (cylinder) to provide a $\frac{11}{32}$-inch step height to aid in the determination of the type of boundary layer that existed on the rearward part of the cylinder. Sketches of the sting, sliding collar, and disk are shown in figure 1(b).

Test Methods and Techniques

The 16 static-pressure orifices on the afterbodies were connected to 4 pressure switching devices which, in turn, connected the orifices in sequence to electrical pressure transducers. Each pressure switching device had a 1 psia and a 5 psia transducer whose electrical output was recorded on a digital read-out system. The accuracies of the 1 psia and 5 psia transducers were better than 1/4 and 1/2 percent, respectively, of the full-scale reading; however, with the exception of the tests employing the disk, only data from the 1 psia transducers were used. All calculations were based on a nominal free-stream Mach number of 5.98. The maximum errors of three representative pressure coefficients are given in the following table:

$C_{p,\infty}$	$\Delta C_{p,\infty}$ due to Mach number	$\Delta C_{p,\infty}$ due to pressure measurements
-0.03	±0.0005	±0.0005
0	±.0008	±.0006
.06	±.0017	±.0009

A prism was attached to the base of the model during preliminary tests and was used with a light source and calibrated screen to obtain true angle of attack in the presence of sting deflections. An angle gage was calibrated during these preliminary tests and was used to set the angles of attack for the remainder of the test program. The angles of attack were set at nominal angles of 0°, 2°, 4°, 6°, 9°, and 12° and are believed to be within ±1/4° of the desired angle.

DATA INTERPRETATION

Cylinder

Mach number.- Calculations by the method of characteristics indicate that the local Mach number at $x'/D = 0$ (cylinder-boattail junction) at $\alpha = 0°$ for the 15° (nose section 1) and 45° (nose section 2) conical nose sections should be 5.82 and 3.75, respectively. For the hemispherical nose section, it was assumed that the total pressure on the cylinder was determined by a normal shock loss and the local pressure was free stream; the resulting theoretical Mach number was 3.16. Mach numbers based on the ratios of the measured static pressures to the theoretical total pressures behind the conical and normal shocks are 5.80, 3.72, and 3.13, respectively, for nose sections 1, 2, and 3. These measured values of cylinder Mach number were used where applicable.

Boundary layer.- The type of boundary layers that existed on the rearward parts of the models at $\alpha = 0°$ was determined by observing the pressures in the separated region forced by a forward-facing step at the rear of the models. (See, for example, refs. 15 to 17.) The pressures in the separated region were assumed to be similar to those for separated flow on a flat plate. Presented in figure 2(a) are the pressure distributions along the cylindrical afterbody ($\beta = 0°$) with the $\frac{11}{32}$-inch step at $x/D = 1.0$. In figure 2(b) three empirical curves for different Mach number ranges and boundary-layer types (eqs. (1), (2), and (5), of ref. 15) are shown which relate the peak pressure rise as a function of Mach number for forward-facing steps in turbulent and laminar boundary-layer flows. (These pressures have been shown to be a very weak function of Reynolds number for turbulent boundary layers. Calculated local Reynolds numbers for the present tests were used in eq. (5) of ref. 15.) A comparison of these curves with the present experimental values from figure 2(a) indicates that the boundary layers were turbulent on the rearward parts of the cylinder for all three nose sections at $\alpha = 0°$. At angles of attack the pressures in the separated region were affected by a strong radial pressure bleed ahead of the step, which

distorted the peak-pressure-rise measurements. Positive identification of the boundary-layer type at angle of attack was not possible; however, it is believed that the boundary layers became transitional or even laminar before separating off the leeward meridians at the higher angles of attack.

Base

Radial location.- Presented in figure 3 are average base pressure coefficients at various radial angles and angles of attack for boattail angles of 0° and 21° (nose section 1). These data are the average of pressure values obtained from orifices 13 and 14 for $\phi = 0^\circ$ and 45°, orifices 13 to 16 for $\phi = 90^\circ$, and orifices 15 and 16 for $\phi = 135^\circ$ and 180°; however, the variation from the average values was negligible. Lines of constant pressure are shown for each angle of attack and the variations of the data from these lines were less than the maximum possible data error. It is believed that for a given test condition the pressures on the entire base were essentially constant and all subsequent data are the average of values obtained from orifices 13 to 16.

Sting effects.- References 1 and 18 indicate that the presence of a model support, no matter how small, affects the base wake structure to some degree; however, the effect upon base pressure is uncertain. Base pressure coefficients for the 0° and 21° boattails with various sting lengths at angles of attack are given in figure 4(a) for a constant sting diameter ($d_s/D = 0.37$). The data showed only a small variation for sting lengths ranging from 1.0 to 3.0 model diameters. In figure 4(b) base pressure coefficients for various sting diameters at angles of attack are presented for a constant sting length ($l_s/D = 2.97$). The pressures appear to become constant for a sting-to-model diameter ratio of less than about 0.4 for both the 0° and 21° boattails. For all subsequent tests the models were supported by a sting with $l_s/D = 2.97$ and $d_s/D = 0.37$, and it is believed that the support interference was negligible.

Reynolds number effects.- Presented in figure 5 are base pressures from preliminary tests (nose section 1, $\beta = 0^\circ$) and from references 1, 9, 14, and 19 as a function of Reynolds number for turbulent boundary layers. (Note that the cone data of reference 19 are plotted as the ratio of the base pressure to the cone surface pressure rather than to the free-stream pressure.) Generally, for Mach numbers greater than about 3 the base pressures decrease with Reynolds number until the boundary layer becomes fully turbulent and then remain approximately constant for further increases in Reynolds number. This constant-pressure condition was attained in the preliminary tests at a Reynolds number of about 10×10^6 and all subsequent tests were conducted at a Reynolds number of 12×10^6 to insure the formation of turbulent boundary layers.

RESULTS AND DISCUSSION

Boattail Pressures

Boattail-pressure distributions.- Presented in figure 6 to 8 are the pressure distributions along the boattail surfaces for nose sections 1 to 3,

respectively, for various boattail and radial angles at angles of attack. The pressures were relatively constant along each of the conical afterbodies for a given test condition particularly at lower angles of attack ($\alpha < 6^\circ$), whereas at higher angles of attack ($\alpha > 6^\circ$) the pressures generally decreased toward the base. Large pressure gradients existed on the circular-arc boattail, which were caused by the continuous expansion of the flow along the curved surface. The circular-arc data are included in some of the figures but primary emphasis is placed on the conical boattail data. At $x/D = 0.408$ a common orifice existed on the cylinder for each of the model configurations and the small differences in pressure which occurred for the various boattails are believed to have been caused by angle-of-attack and data errors and not by boattail-angle effects.

Prediction of boattail pressures.- Presented in figure 9 are the pressure distributions along the boattail surfaces at zero angle of attack, replotted from figures 6(a), 7(a), and 8(a) with the ordinate and abscissa converted, respectively, from $C_{p,\infty}$ to P_{bt}/P_c and x/D to x'/D. Boattail pressure distributions calculated by the method of characteristics are shown for boattail angles of 6°, 12°, and 18° at cylinder Mach numbers of 3.13 and 5.80 which were the minimum and maximum measured Mach numbers at $\alpha = 0^\circ$ for the present tests. (Calculations were begun at the boattail-cylinder junction, assuming the Mach number was constant, vertically, at this point.) The characteristics method grossly underpredicts the pressure data and indicates that the pressure ratio should decrease sharply with cylinder Mach number - a trend which was not found experimentally. Instead, the trends and magnitudes of the pressure ratios were almost the same for each nose section at a given boattail angle. Included in figure 9 are pressure distributions calculated by Van Dyke's second-order theory (ref. 20) as applied to conical boattails by Jack (ref. 21) for $\beta = 6^\circ$ and 12° at $M_c = 3.13$. This theory also underpredicts the data.

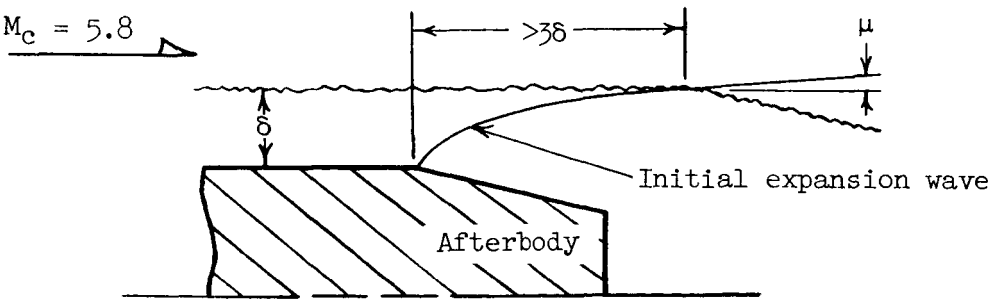

Sketch 1

In sketch 1 a typical afterbody, boundary layer, and initial expansion wave are shown to scale, based upon measurements from schlieren photographs of the present tests (nose section 1, $\alpha = 0^\circ$, $M_c = 5.80$). The initial expansion wave intersects the inviscid outer flow more than 3 boundary-layer thicknesses downstream of the cylinder-boattail junction, the intersection being aft of the base.

Inviscid prediction methods are based upon the Mach number of the outer flow; therefore, it should be expected that they would not be applicable for short boattails with thick boundary layers.

In figure 10(a) ratios of the average boattail surface pressure to the cylinder pressure are given as a function of boattail angle at $\alpha = 0^{\circ}$. Values of p_{bt}/p_c calculated by the two-dimensional Prandtl-Meyer expansion method for $M_c = 1.00$, 3.13, and 5.80 are also shown. (The characteristics method reduces to the Prandtl-Meyer method at $x'/D = +0.0$.) An inspection of figure 10(a) reveals that all the present data are in good agreement with the sonic expansion curve, whereas the two curves calculated from the measured cylinder Mach numbers generally underpredict the data by a large margin. Included in this figure are two-dimensional boattail data from references 22 and 23, which are also in good agreement with the sonic expansion curve for $\beta \leqq 12^{\circ}$. (The flow separated from the boattail surface at $\beta > 12^{\circ}$ (ref. 22).)

Presented in figures 10(b) and 10(c) are average boattail-to-cylinder pressure ratios at angles of attack of 6° and 12°, respectively, and included are two-dimensional data of reference 22. Calculated curves of p_{bt}/p_c for $M_c = 3.0$ and 6.3 at $\alpha = 6^{\circ}$ and $M_c = 2.6$ and 6.8 at $\alpha = 12^{\circ}$ are shown with the sonic expansion curve for comparison. (At $\alpha = 6^{\circ}$ and 12°, cylinder Mach numbers of 3.0 and 2.6 and of 6.3 and 6.8 were the minimum and maximum, respectively. These Mach numbers were based on measured cylinder static pressures and total pressures behind normal (hemispherical nose section) and oblique (15° conical nose section) shocks. (See ref. 24.) An inspection of figures 10(b) and 10(c) reveals that the data tend to center about the sonic expansion curve rather than lie within the maximum and minimum Mach number curves. The two-dimensional data are again in good agreement with the sonic expansion curve ($\beta \leqq 12^{\circ}$) and show very little variation of pressure ratio with angle of attack because these boattails are not susceptible to cross-flow bleed as are conical boattails. (The variation of the pressure ratios with radial angle is believed to have been caused by cross-flow bleeding of the higher windward pressures to the leeward surface.) The apparent success of the sonic-expansion method in figures 9 and 10 may be fortuitous; however, a possible explanation for its validity is offered.

The expansion of a supersonic boundary layer around a corner is followed by a decrease in the boundary-layer pressure and density and an increase in thickness which is consistent with mass conservation requirements (sketch 2).

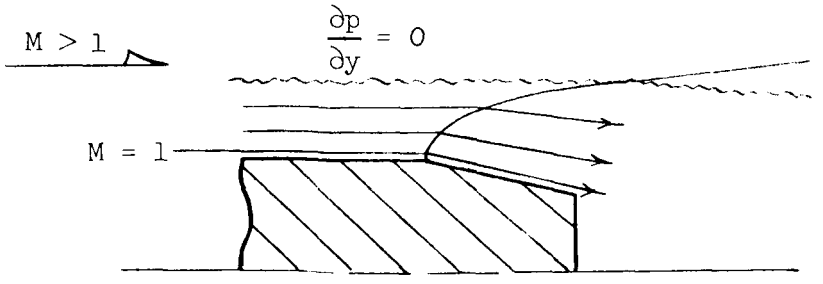

Sketch 2

The inner streamlines are expected to conform to the body contour because of their lower velocity and total pressure, whereas the outer streamlines of the boundary layer would diverge from the body surface in the region immediately aft of the corner. This type of process would be favorable to establish a zero pressure gradient ($\partial p/\partial y = 0$) in the expanded boundary layer. Experimental data of reference 15 indicate that the sonic streamlines of the turbulent boundary layer ($M_c = 5.8$) occurred approximately 0.03δ from the plate. During an expansion process streamlines in this region of the boundary layer must expand essentially parallel to the body contour when separation does not occur. The pressures on the body surface for some distance downstream from the corner would then be determined by the expansion of a sonic flow through the turning angle ($\beta = \nu$).

At a lower Mach number the sonic streamline occurs at a relatively higher position in the boundary layer and would not necessarily expand parallel to the body. Also, the initial expansion wave will intersect the inviscid flow nearer to the corner which would allow inviscid prediction methods to be more applicable. In figure 11 boattail pressure distributions from references 11, 13, and 25 are presented and are compared with those obtained by Van Dyke's second-order theory and the sonic-expansion method. The second-order theory gave a good overall prediction of the boattail pressures especially at the lower Mach numbers. The sonic-expansion method was generally better at the higher Mach numbers for some distance aft of the cylinder-boattail junction with the second-order theory showing better agreement at the aft end of the boattail. It is concluded that the second-order theory is most applicable for long boattails with thin boundary layers at low Mach numbers, whereas the sonic-expansion method is most applicable for short boattails with thick boundary layers at high Mach numbers.

Base Pressures

Effect of boattailing.- Presented in figure 12 are the base pressure coefficients as a function of boattail angle for nose sections 1, 2, and 3 at various angles of attack. For each nose section and angle of attack, the base pressure has a maximum value at a boattail angle between 12° and 18°. A comparison of the pressures on the base (fig. 12) and trailing edge (figs. 6 to 8) of the 18° and 21° boattails show that the pressures are essentially equal and indicate that the flow had separated from these boattail surfaces. For very large boattail angles ($\beta > 30^\circ$), it is expected that the separated flow would not sense the existence of the afterbody and that the base and boattail pressures could be closely approximated by the $\beta = 0^\circ$ base pressure (sketch 3).

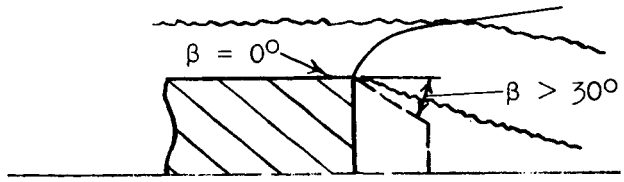

Sketch 3

Presented in figure 13 is a compilation of base-pressure data from references 2, 9, 10, 13, and 26 for boattailed bodies of revolution with turbulent boundary layers for cylinder Mach numbers between 1.5 and 6.0. With the exception of the hemispherical nose section of the present tests (solid symbols), all the models had either ogive or conical nose sections and were from 5 to 12 cylinder diameters in length. The base pressures are plotted in ratio to the cylinder pressure at the cylinder-afterbody junction in order to reduce the effects of nose and cylinder length. If experimental cylinder pressures were not available, they were estimated by the method of reference 27 and these estimated pressures were used to calculate the local cylinder Mach number. From cross plots of these data, lines of constant cylinder Mach number were determined and are shown as faired curves. All data for bodies with pointed nose shapes agree reasonably well with the correlated curves throughout the Mach number and boattail-angle ranges of the compiled data. However, the base pressures for the hemisphere-cylinder (solid symbols) are overestimated by the correlation ($M_c = 3.13$) and apparently nose effects were not eliminated for this configuration.

Comparisons with two-dimensional pressure data.- In figure 14(a) the present data (nose section 1) are compared with the two-dimensional pressure data of reference 22 at $\alpha = 0^\circ$, which were also obtained in the Langley 20-inch Mach 6 tunnel. These data, in particular, are comparable in that the model and afterbody profiles and test conditions were similar. The base pressure coefficients for both configurations increase almost linearly with boattail angle from $\beta = 0^\circ$ to 12°, and the base pressure coefficients for the two-dimensional body are about 0.007 greater than those of the present three-dimensional body. Separation of the flow from the surfaces of the $\beta = 15^\circ$ two-dimensional afterbody resulted in a sharp decrease in base pressure to a value nearly equal to that for $\beta = 0^\circ$. For the present tests the flow separated from the $\beta = 18^\circ$ conical afterbody which, similarly, resulted in a decrease of base pressure. From the foregoing statements it might be inferred that afterbody flow separation is the primary cause of the decrease in base pressure after the initial increase which occurs for conical boattail angles between about 14° and 18° at cylinder Mach numbers from 1.5 to 6.0 (fig. 13.)

Presented in figure 14(b) are faired curves of compiled base pressure data ($\beta = 0^\circ$, fig. 13) for bodies of revolution and two-dimensional bodies (ref. 22) as a function of Mach number. The base pressures on bodies of revolution are higher than those on two-dimensional bodies for $M_c < 3.6$, whereas the reverse is true at higher Mach numbers. A pressure coefficient of $\frac{-1}{M_c^2}$ is often used as a base-pressure correction factor for the reduction of supersonic force data when base pressures are not measured. It is seen that the $\frac{-1}{M_c^2}$ curve is in good agreement with the two-dimensional data for $M_c > 1.8$ and with the body-of-revolution data for $M_c > 3.0$. For most general applications $\frac{-1}{M_c^2}$ can serve as an easy-to-compute estimate of the base pressure coefficient for bodies with turbulent boundary layers at high Mach numbers.

Effect of angle of attack.- In reference 25 it is reported that the initial effect of angle of attack was to cause a decrease in base pressure until separation on the leeward surface becomes appreciable and that further increases in angle of attack would cause a slight increase in base pressure (the angle of attack for flow separation on the leeward surface generally decreases with increasing Mach number). In figure 15 the effect of angle of attack on base pressure is shown for various bodies of revolution for $\beta = 0^{\circ}$; the data are consistent with the trends of reference 25. The present data decrease to a minimum pressure of about 75 percent of that at $\alpha = 0^{\circ}$ at angles of attack between 6° and 12° depending on the nose shape. The angles of attack for the reference data apparently were not sufficiently high to cause separation.

Review of prediction methods.- In the past two decades many methods have been proposed for predicting base pressure on bodies of revolution at supersonic speeds. Theoretical methods presented in references 2, 28, and 29 generally give correct qualitative values; however, they have not been found to be suitable quantitatively. Empirical or semiempirical methods given in references 1, 10, 25, and 30 to 33 are dependent upon experimental measurements and generally give satisfactory results when applied within their intended limits. Methods for predicting base pressure on boattailed bodies are presented in references 1 and 10 and were found to be only in qualitative agreement with the present correlation. In reference 25 a means for estimating the base pressure on bodies of revolution at angles of attack is given which was in fair agreement with the experimental data of reference 34 ($M_{\infty} = 1.49$). The applicability of this method at higher Mach numbers is not known.

It has been shown by previous investigators (refs. 1, 10, and 25, for example) that the parameters which determine base pressure are: free-stream Mach number and Reynolds number, nose shape, body length, boattail angle and length, boundary-layer type, and angle of attack. Free-stream Mach number, nose shape (attached shock), and body length can generally be reduced to cylinder Mach number, and the free-stream Reynolds number and body length can be reduced to boundary-layer thickness. For bodies of revolution with fully developed turbulent boundary layers at zero angle of attack, the remaining variables are: cylinder Mach number M_c, boattail angle β and length l_{bt}/D, and boundary-layer thickness δ/D.

The lack of sufficient data limited the present correlation (fig. 13) to the evaluation of cylinder Mach number and boattail-angle effects, which were determined independent of the boundary-layer-thickness and boattail-length effects. For turbulent boundary layers the effects of δ/D and l_{bt}/D can be quite large (refs. 9 and 10, for example) if these parameters are allowed to vary over a wide range of values. However, the fact that all data of the present correlation agreed reasonably well with the faired curves indicates that such effects were probably small.

It is concluded from a review of previous investigations that no comprehensive theoretical methods exist for predicting quantitative values of base pressure as a function of its known variables. Base-pressure data are available for a wide range of parameters, which make possible reasonable estimates for most practical applications as is the intention of the present correlation in figure 13. However, if one or more of the primary variables of an investigation

are radically different from those of the data used as a basis, the application of the present correlation could be greatly in error.

Afterbody Drag

Presented in figure 16 are the components of axial-force coefficient due to afterbody pressure drag, which were obtained from integration of the experimental pressures over the boattail and base surfaces. At all angles of attack minimum afterbody drag could be obtained with about a 13° boattail angle for nose section 1 and between $\beta = 9^\circ$ and 12° for nose sections 2 and 3 at $\alpha = 0^\circ$. Afterbody drag was reduced 17 to 26 percent (depending upon nose shape) at $\alpha = 0^\circ$ as the result of boattailing the afterbody 12° but was increased as much as 5 percent ($\beta = 0^\circ$) to 12 percent ($\beta = 12^\circ$) at angle of attack. Although only one circular-arc boattail was tested, the afterbody drag for this configuration was only slightly higher than the minimum conical boattail drag and perhaps circular-arc boattails should receive primary attention in future studies.

Calculated values of afterbody pressure drag are given in figure 17 as a function of boattail angle, Mach number, and boattail length. These coefficients were calculated by use of Van Dyke's second-order theory (see ref. 21) and the sonic-expansion method to estimate boattail drag, and the base-pressure correlation curves of figure 13 were used to estimate base drag. The calculated afterbody drag decreases initially with an increase in boattail angle and, for the cases shown, reaches a minimum value between $\beta = 5^\circ$ and 13° which is dependent upon Mach number and boattail length. At the lower Mach numbers minimum drag is sensitive to boattail angle, whereas at the higher Mach numbers a near minimum drag can be obtained with a boattail angle $\pm 4^\circ$ from the boattail angle at which minimum afterbody drag occurred β_{min}.

Minimum afterbody drag coefficients and their associated boattail angles are compared to values of afterbody drag for $\beta = 0^\circ$ in figure 18. (These curves were obtained from figure 17 and similar curves calculated at Mach numbers of 1.5, 2.5, and 3.5.) These calculated curves show that afterbody pressure drag can be reduced about 36 percent at Mach numbers around 2.3 for a boattail length l_{bt}/D of 1.00 and for even a relatively short boattail ($l_{bt}/D = 0.35$) a reduction in afterbody drag between 20 and 32 percent can be obtained in the Mach number range from 1.5 to 6.0. The boattail angle necessary to obtain minimum drag β_{min} decreases with an increase in boattail length and generally increases with increasing Mach number toward an asymptotic value. Skin friction was not considered in the preceding calculations because its effect upon general trends, β_{min}, and afterbody drag reduction were found to be negligible for most practical applications. Calculations of the skin-friction drag on the $\beta = 0^\circ$ and 12° boattails (nose section 1) by the Monaghan T' method (see ref. 35) with near adiabatic wall conditions gave values of 0.0011 and 0.0009, respectively. These values are about 3 percent of the afterbody pressure drag (fig. 16) and therefore were neglected.

CONCLUDING REMARKS

Afterbody pressures have been investigated at a free-stream Mach number of 5.98 on various boattailed bodies of revolution at angles of attack. The Reynolds number and roughness bands were sufficient to cause a turbulent boundary layer to exist ahead of the afterbodies at zero angle of attack. A simple method for predicting two-dimensional and axisymmetric boattail pressures at high Mach numbers is presented, which gave a good estimate of the present data at zero angle of attack. A correlation of existing base-pressure data (zero angle of attack) was made for bodies of revolution with various boattails and turbulent boundary layers between cylinder Mach numbers of 1.5 and 6.0. Cylinder Mach number and boattail angle were found to be the two primary variables affecting base pressure for bodies with attached shocks.

The present tests show that afterbody pressure drag can be reduced from 17 to 26 percent with use of a relatively short 12° conical boattail, whereas calculations indicate that reductions of about 36 percent can be realized at Mach numbers around 2.3. The boattail angle necessary to obtain minimum drag increases with increasing Mach number and decreases with an increase in boattail length.

Langley Research Center,
National Aeronautics and Space Administration,
Langley Station, Hampton, Va., December 10, 1964.

REFERENCES

1. Chapman, Dean R.: An Analysis of Base Pressure at Supersonic Velocities and Comparison With Experiment. NACA Rept. 1051, 1951. (Supersedes NACA TN 2137.)

2. Kurzweg, H. H.: Interrelationship Between Boundary Layer and Base Pressure. J. Aeron. Sci., vol. 18, no. 11, Nov. 1951, pp. 743-748.

3. Faro, I. D. V.: Experimental Determination of Base Pressures at Supersonic Velocities. Bumblebee Rept. No. 106, The Johns Hopkins Univ., Appl. Phys. Lab., Nov. 1949.

4. Van Hise, Vernon: Investigation of Variation in Base Pressure Over the Reynolds Number Range in Which Wake Transition Occurs for Nonlifting Bodies of Revolution at Mach Numbers From 1.62 to 2.62. NACA TN 3942, 1957.

5. Potter, J. L.: Friction Drag and Transition Reynolds Number on Bodies of Revolution at Supersonic Speeds. NAVORD Rept. 2150, U.S. Naval Ord. Lab. (White Oak, Md.), Aug. 20, 1950.

6. Hastings, R. C.: A Note on the Interpretation of Base Pressure Measurements in Supersonic Flows. C.P. No. 409, Brit. A.R.C., 1958.

7. Charczenko, Nickolai; and Hayes, Clyde: Jet Effects at Supersonic Speeds on Base and Afterbody Pressures of a Missile Model Having Single and Multiple Jets. NASA TN D-2046, 1963.

8. Brazzel, Charles E.: The Effects of Base Bleed and Sustainer Rocket Nozzle Diameter and Location on the Base Drag of a Body of Revolution With Concentric Boost and Sustainer Rocket Nozzles. Rept. No. RF-TR-63-23, U.S. Army Missile Command (Redstone, Arsenal, Ala.), July 15, 1963.

9. Reller, John O., Jr.; and Hamaker, Frank M.: An Experimental Investigation of the Base Pressure Characteristics of Nonlifting Bodies of Revolution at Mach Numbers From 2.73 to 4.98. NACA TN 3393, 1955. (Supersedes NACA RM A52E20.)

10. Cortright, Edgar M., Jr.; and Schroeder, Albert H.: Investigation at Mach Number 1.91 of Side and Base Pressure Distributions Over Conical Boattails Without and With Jet Flow Issuing From Base. NACA RM E51F26, 1951.

11. Maxwell, N. E.; and Shutts, W. H.: Aerodynamic Effects of Boattailing on a Body of Revolution - Mach Numbers 1.5, 2.0 & 2.5. Rept. No. CM-645 (Contract No. NORD 9028), Consolidated Vultee Aircraft Corp., Mar. 15, 1951.

12. Katz, Ellis; and Stoney, William E., Jr.: Base Pressures Measured on Several Parabolic-Arc Bodies of Revolution in Free Flight at Mach Numbers From 0.8 to 1.4 and at Large Reynolds Numbers. NACA RM L51F29, 1951.

13. Baughman, L. Eugene; and Kochendorfer, Fred D.: Jet Effects on Base Pressures of Conical Afterbodies at Mach 1.91 and 3.12. NACA RM E57E06, 1957.

14. Bogdonoff, Seymour M.: A Preliminary Study of Reynolds Number Effects on Base Pressure at M = 2.95. J. Aeron. Sci., vol. 19, no. 3, Mar. 1952, pp. 201-206.

15. Sterrett, James R.; and Emery, James C.: Extension of Boundary-Layer-Separation Criteria to a Mach Number of 6.5 by Utilizing Flat Plates With Forward-Facing Steps. NASA TN D-618, 1960.

16. Love, Eugene S.: Pressure Rise Associated With Shock-Induced Boundary-Layer Separation. NACA TN 3601, 1955.

17. Chapman, Dean R.; Kuehn, Donald M.; and Larson, Howard K.: Investigation of Separated Flows in Supersonic and Subsonic Streams With Emphasis on the Effect of Transition. NACA Rept. 1356, 1958. (Supersedes NACA TN 3869.)

18. Dayman, Bain, Jr.: Optical Free-Flight Wake Studies. Tech. Rept. No. 32-364 (Contract No. NAS 7-100), Jet Propulsion Lab., C.I.T., Nov. 1, 1962.

19. Whitfield, Jack D.; and Potter, J. Leith: On Base Pressures at High Reynolds Numbers and Hypersonic Mach Numbers. AEDC-TN-60-61, U.S. Air Force, Mar., 1960.

20. Van Dyke, Milton D.: Practical Calculation of Second-Order Supersonic Flow Past Nonlifting Bodies of Revolution. NACA TN 2744, 1952.

21. Jack, John R.: Theoretical Pressure Distributions and Wave Drags for Conical Boattails. NACA TN 2972, 1953.

22. Staylor, W. Frank; and Goldberg, Theodore J.: Afterbody Pressures on Two-Dimensional Boattailed Bodies Having Turbulent Boundary Layers At Mach 5.98. NASA TN D-2350, 1964.

23. Fuller, L.; and Reid, J.: Experiments on Two-Dimensional Base Flow at M = 2.4. R. & M. No. 3064, Brit. A.R.C., 1958.

24. Sims, Joseph L.: Tables for Supersonic Flow Around Right Circular Cones at Small Angle of Attack. NASA SP-3007, 1964.

25. Love, Eugene S.: Base Pressure at Supersonic Speeds on Two-Dimensional Airfoils and on Bodies of Revolution With and Without Fins Having Turbulent Boundary Layers. NACA TN 3819, 1957. (Supersedes NACA RM L53C02.)

26. Love, Eugene S; and O'Donnell, Robert M.: Investigations at Supersonic Speeds of the Base Pressure on Bodies of Revolution With and Without Sweptback Stabilizing Fins. NACA RM L52J21a, 1952.

27. Clippinger, R. F.; Giese, J. H.; and Carter, W. C.: Tables of Supersonic Flows About Cone Cylinders. Part I: Surface Data. Rept. No. 729, Ballistic Res. Labs., Aberdeen Proving Ground, July 1950.

28. Crocco, Luigi; and Lees, Lester: A Mixing Theory for the Interaction Between Dissipative Flows and Nearly-Isentropic Streams. Rept. No. 187, Aeron. Eng. Lab., Princeton Univ., Jan. 15, 1952.

29. Davis, Dale D.: Extension of Simplified Mixing Theory to Axially Symmetric Supersonic Wake Flows and Application to the Base Pressure Problem for a Body of Revolution. Rept. 205, Aeron. Eng. Lab., Princeton Univ., May 1953.

30. Gabeaud, A.: Base Pressures at Supersonic Velocities. J. Aeron. Sci. (Readers' Forum), vol. 17, no. 8, Aug. 1950, pp. 525-526.

31. Cope, W. F.: A Comparison of Calculated and Measured Base Pressures of Cylindrically Based Projectiles. C.P. No. 118, Brit. A.R.C., 1953.

32. Korst, H. H.; Page, R. H.; and Childs, M. E.: A Theory for Base Pressures in Transonic and Supersonic Flow. ME Tech. Note 392-2 (Contract No. AF 18(600)-392), Eng. Expt. Sta., Univ. of Illinois, Mar. 1955.

33. Hill, Freeman K.: Base Pressures at Supersonic Velocities. J. Aeron. Sci. (Readers' Forum), vol. 17, no. 3, Mar. 1950, pp. 185-187.

34. Luidens, Roger W.; and Simon, Paul C.: Aerodynamic Characteristics of NACA RM-10 Missile in 8- by 6-Foot Supersonic Wind Tunnel at Mach Numbers From 1.49 to 1.98. I - Presentation and Analysis of Pressure Measurements (Stabilizing Fins Removed). NACA RM E50D10, 1950.

35. Peterson, John B., Jr.: A Comparison of Experimental and Theoretical Results for the Compressible Turbulent-Boundary-Layer Skin Friction With Zero Pressure Gradient. NASA TN D-1795, 1963.

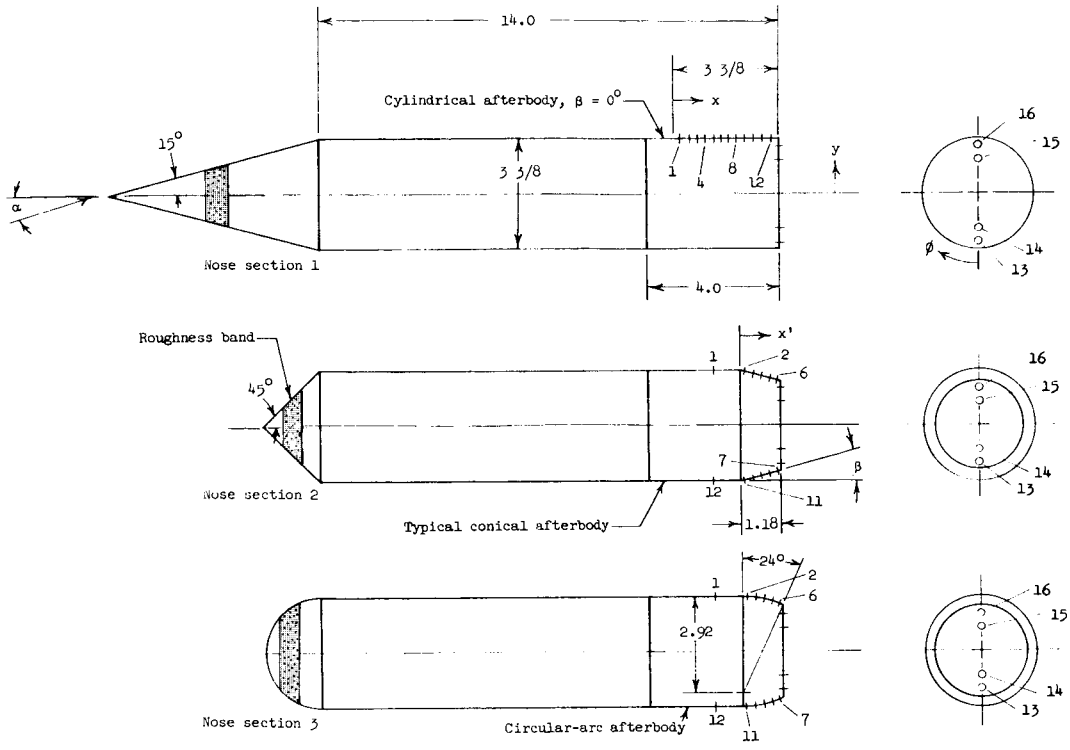

Orifice \ β	0	3	6	9	12	15	18	21	C.A.
					x/D				
1	0.030	0.408	0.408	0.408	0.408	0.408	0.408	0.408	0.408
2	.260	.708	.709	.712	.715	.716	.722	.726	.709
3	.408	.764	.765	.767	.771	.772	.777	.781	.769
4	.467	.821	.822	.823	.825	.827	.833	.835	.829
5	.526	.878	.879	.880	.881	.882	.889	.890	.887
6	.585	.936	.936	.936	.937	.937	.944	.945	.944
7	.644	.936	.936	.936	.937	.937	.944	.945	.944
8	.704	.878	.879	.880	.881	.882	.889	.890	.887
9	.763	.821	.822	.823	.825	.827	.833	.835	.829
10	.822	.764	.765	.767	.771	.772	.777	.781	.769
11	.881	.708	.709	.712	.715	.716	.722	.726	.709
12	.940	.408	.408	.408	.408	.408	.408	.408	.408
					y/D (x/D = 1.000)				
13	0.430	0.398	0.398	0.385	0.370	0.370	0.370	0.361	0.370
14	.383	.352	.352	.352	.352	.352	.352	.315	.315
15	-.383	-.352	-.352	-.352	-.352	-.352	-.352	-.315	-.315
16	-.430	-.398	-.398	-.385	-.370	-.370	-.370	-.361	-.370

(a) Description of models and table of orifice locations.

Figure 1.- Description of models and sting apparatus. All linear dimensions are in inches.

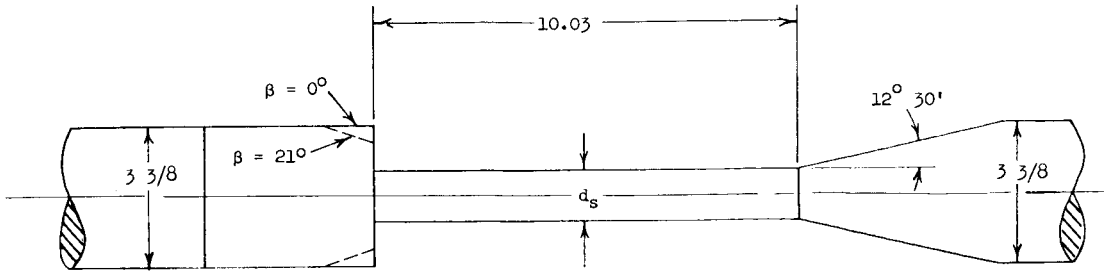

β	l_s/D	d_s/D					
0°	2.97	0.250	0.341	0.370	0.445	0.518	0.575
21°	2.97	0.250	0.341	0.370	0.445	0.518	0.575

Sting

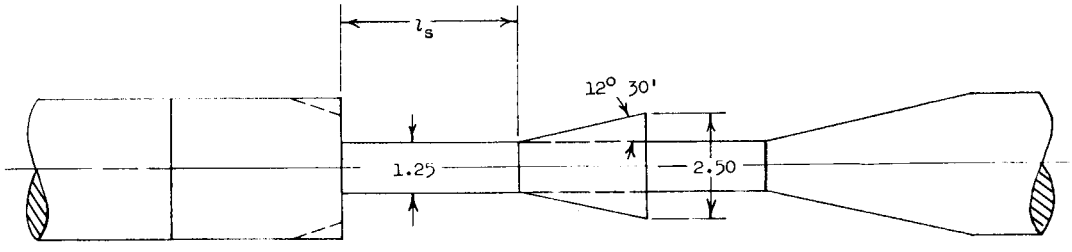

β	d_s/D	l_s/D			
0°	0.370	1.40	1.75	2.32	2.97
21°	0.370	1.00	1.40	2.32	2.97

Sliding collar

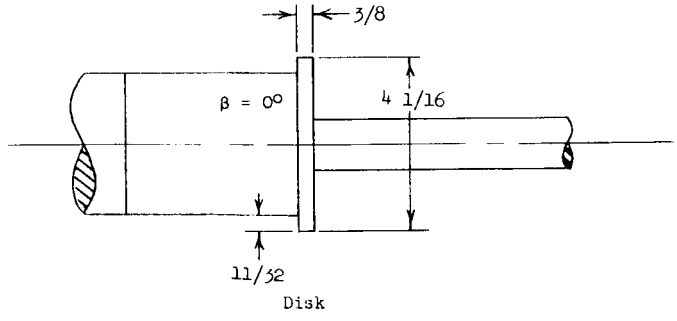

Disk

(b) Description of sting apparatus.

Figure 1.- Concluded.

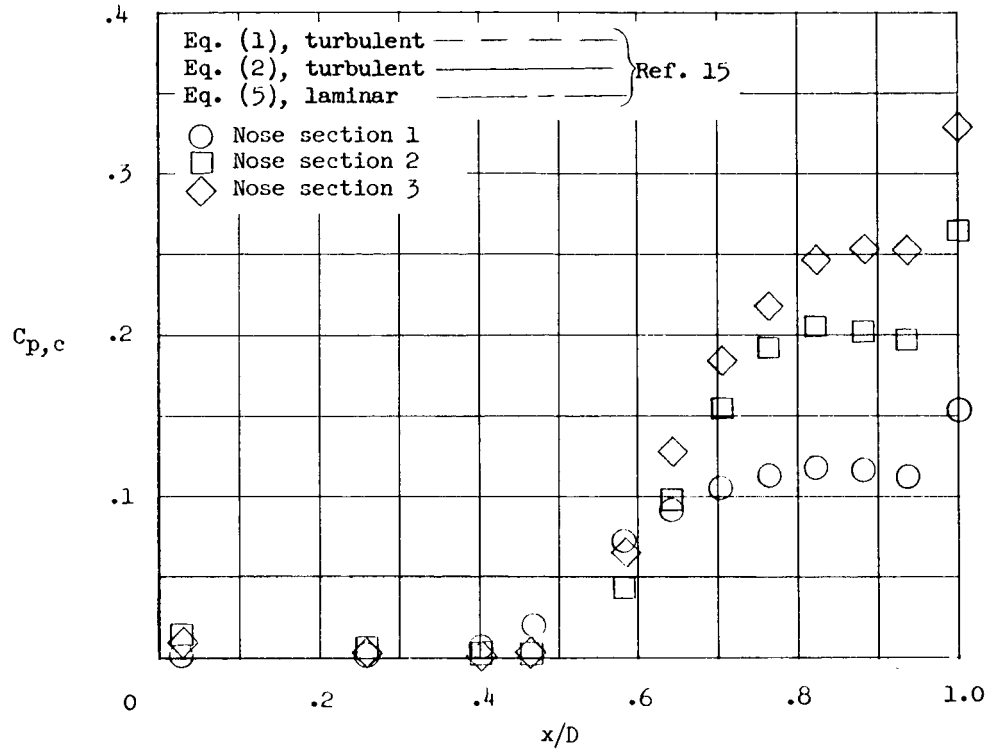

(a) Pressure distribution.

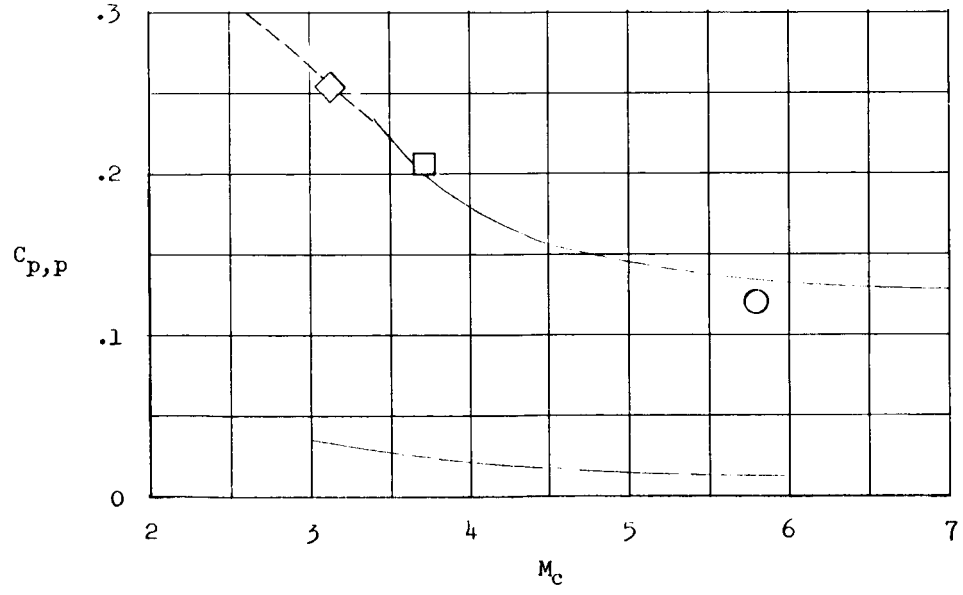

(b) First peak pressure rise.

Figure 2.- Pressure rise ahead of a forward-facing step at $\alpha = 0^\circ$.

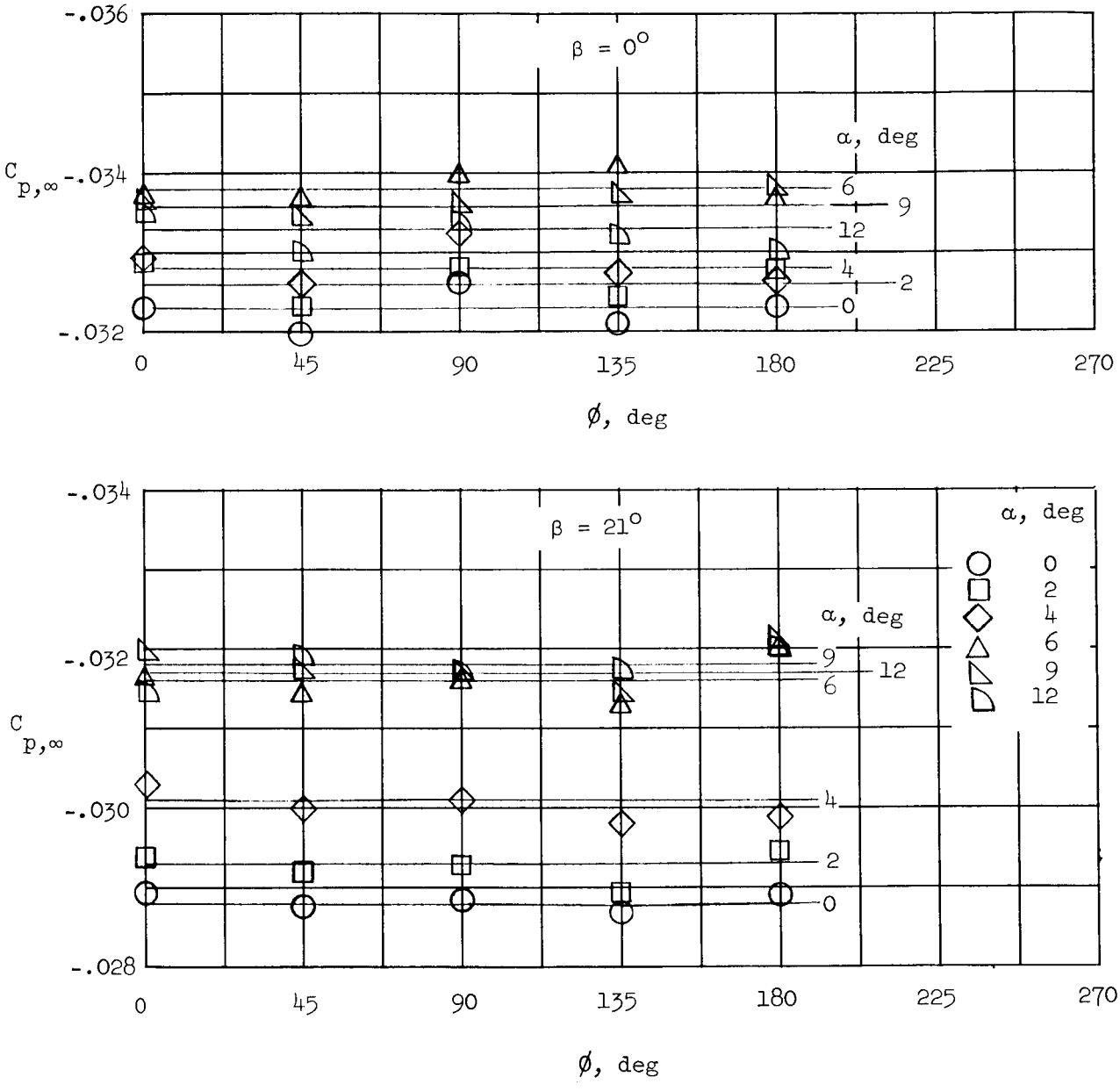

Figure 3.- Variation of base pressure coefficient with radial angle.

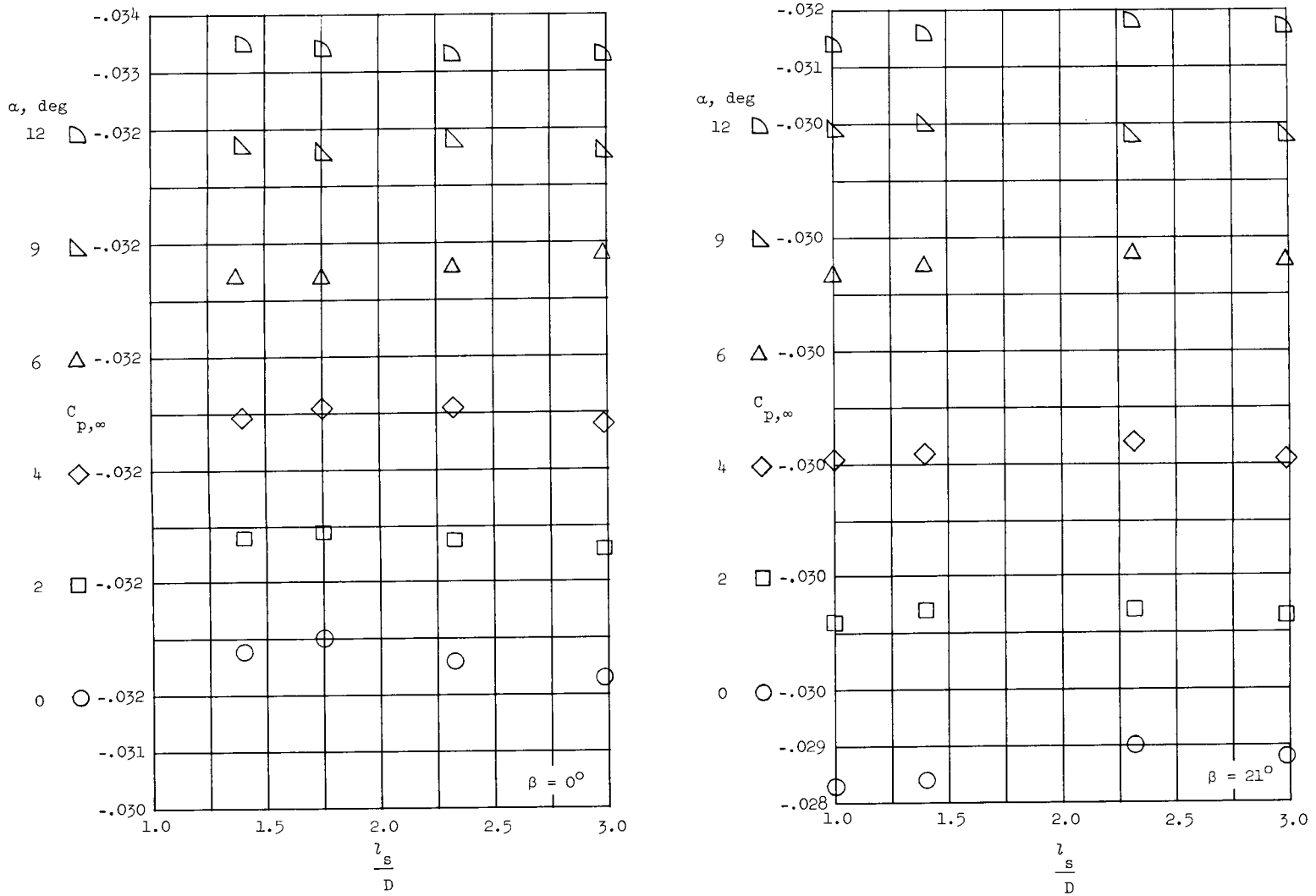

(a) Sting-length effects. $d_s/D = 0.37$.

Figure 4.- Effect of sting length and diameter on base pressure coefficient at various angles of attack. $\beta = 0^\circ$ and 21°; nose section 1.

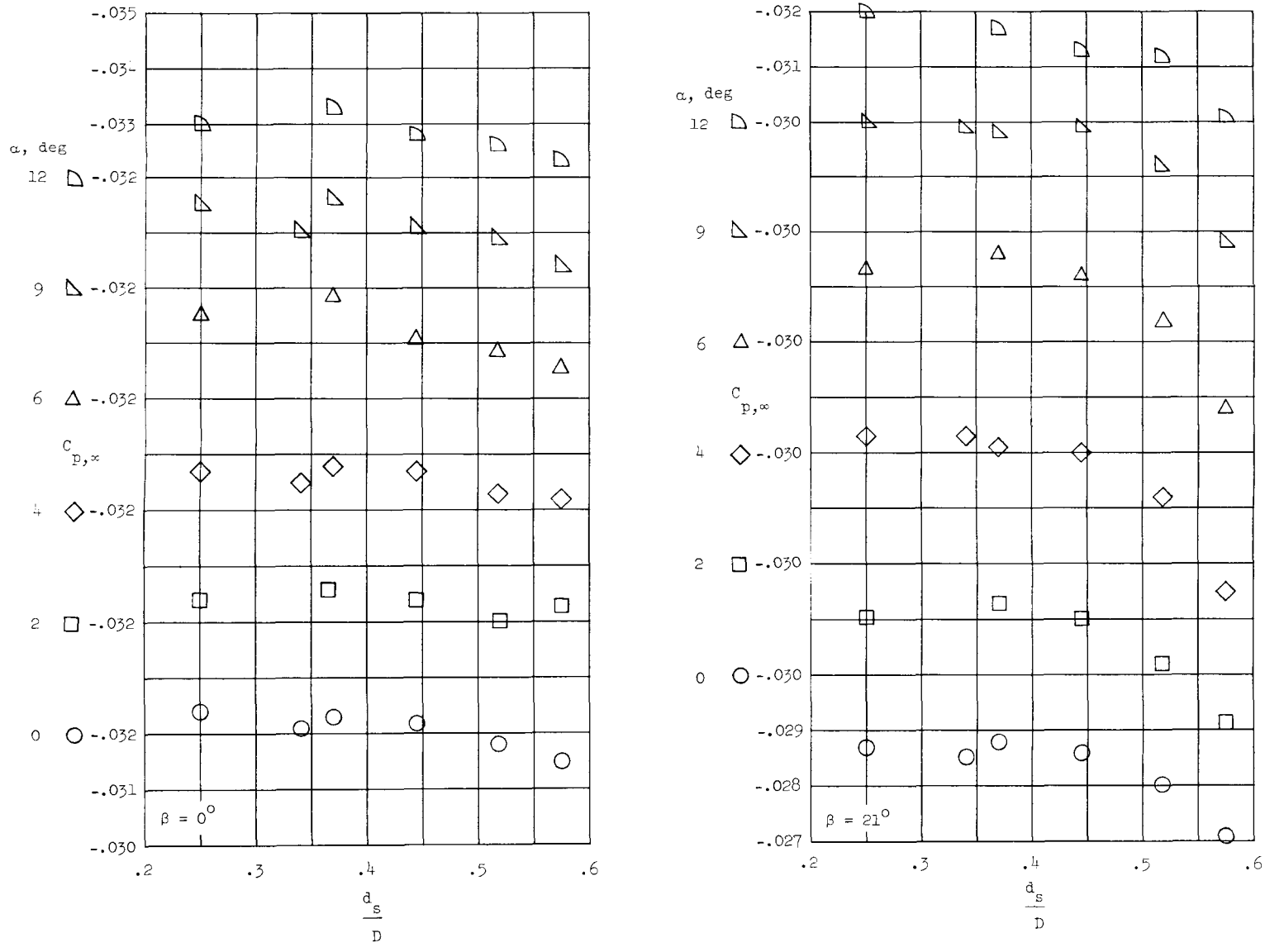

(b) Sting-diameter effects. $l_s/D = 2.97$.

Figure 4.- Concluded.

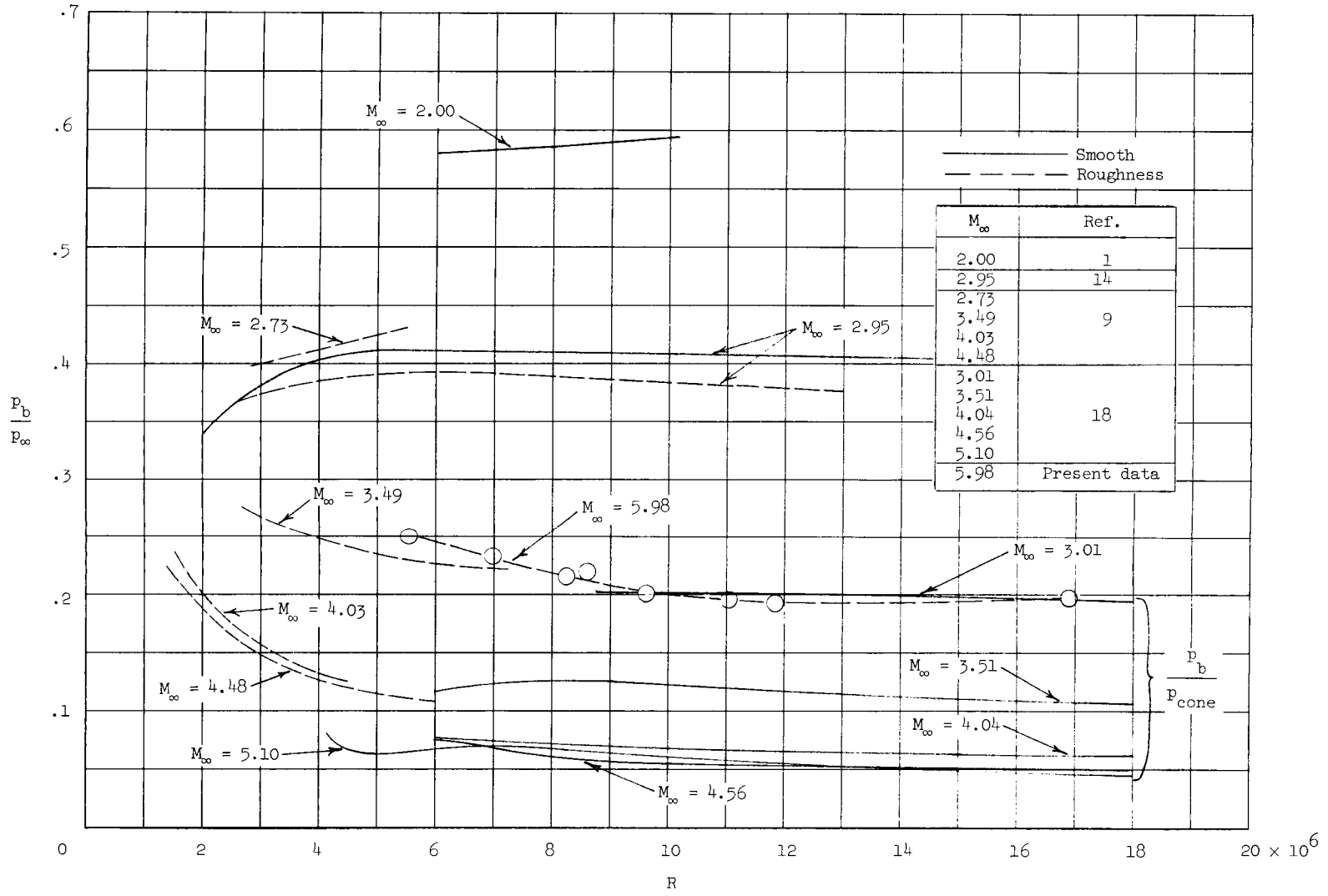

Figure 5.- Effect of Reynolds number on base pressure for bodies of revolution with turbulent boundary layers. $\alpha = 0^\circ$.

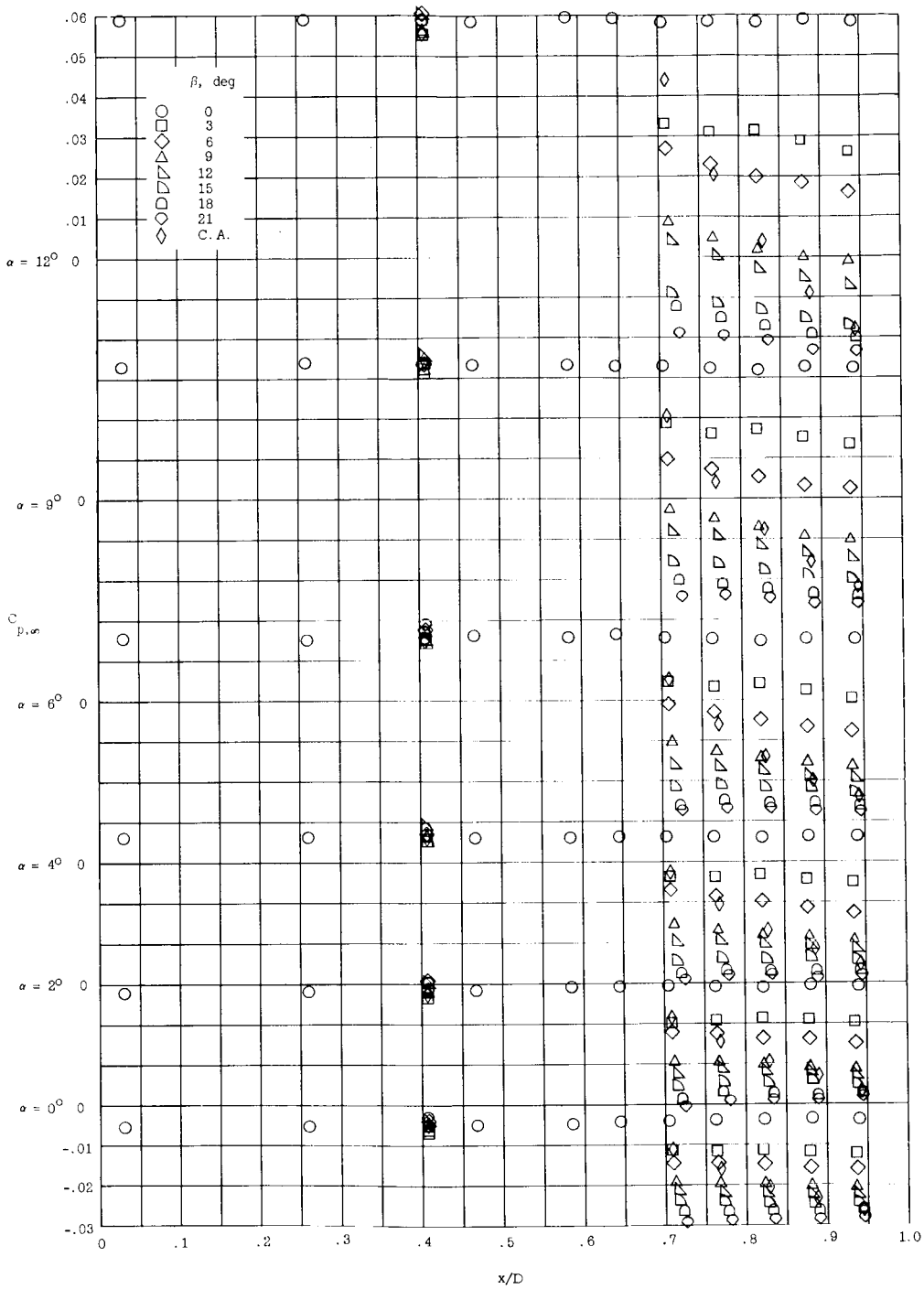

(a) $\phi = 0°$.

Figure 6.- Pressure distribution along the cylinder and afterbody for 15° conical nose section.

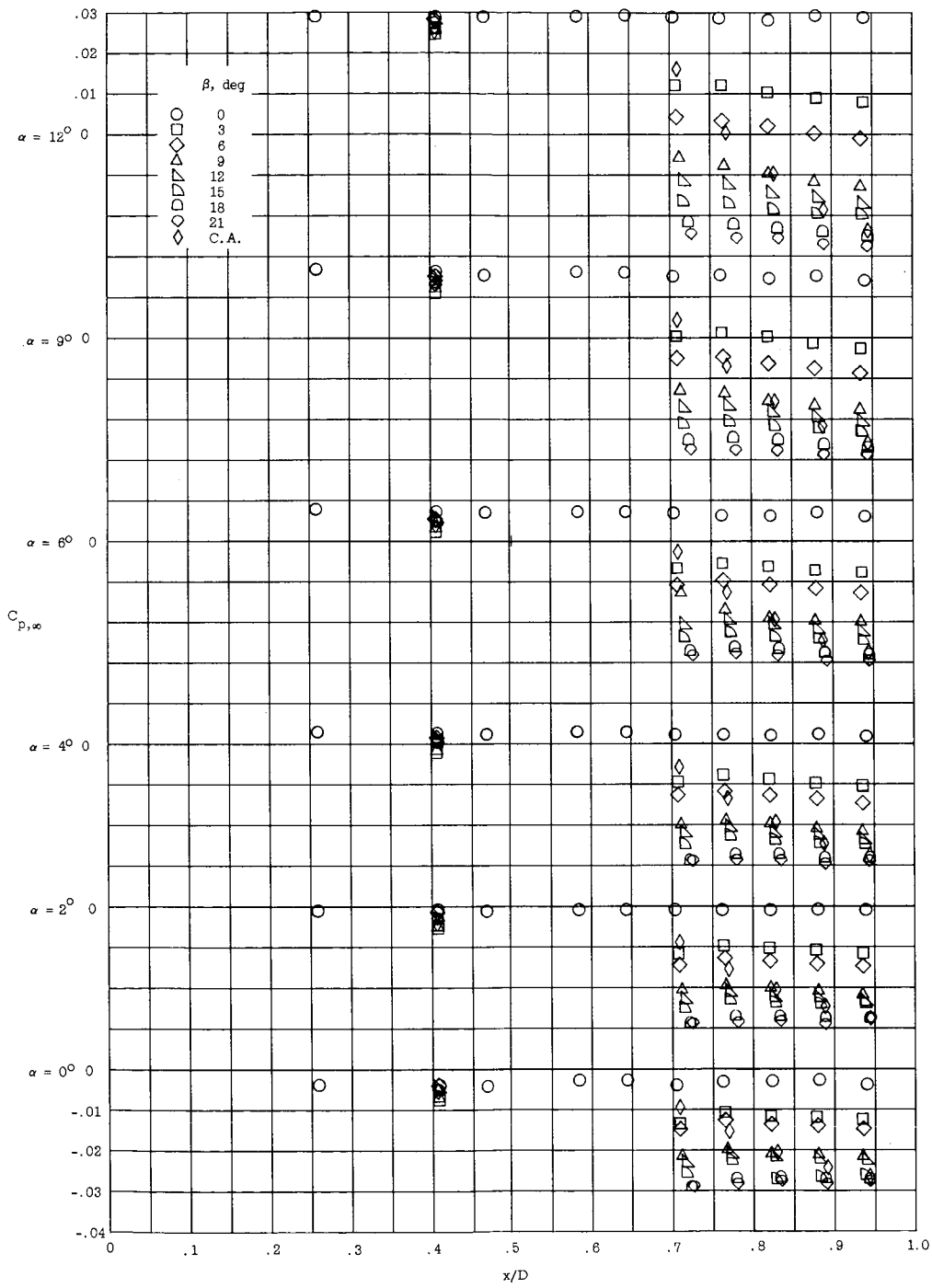

(b) $\phi = 45°$.

Figure 6.- Continued.

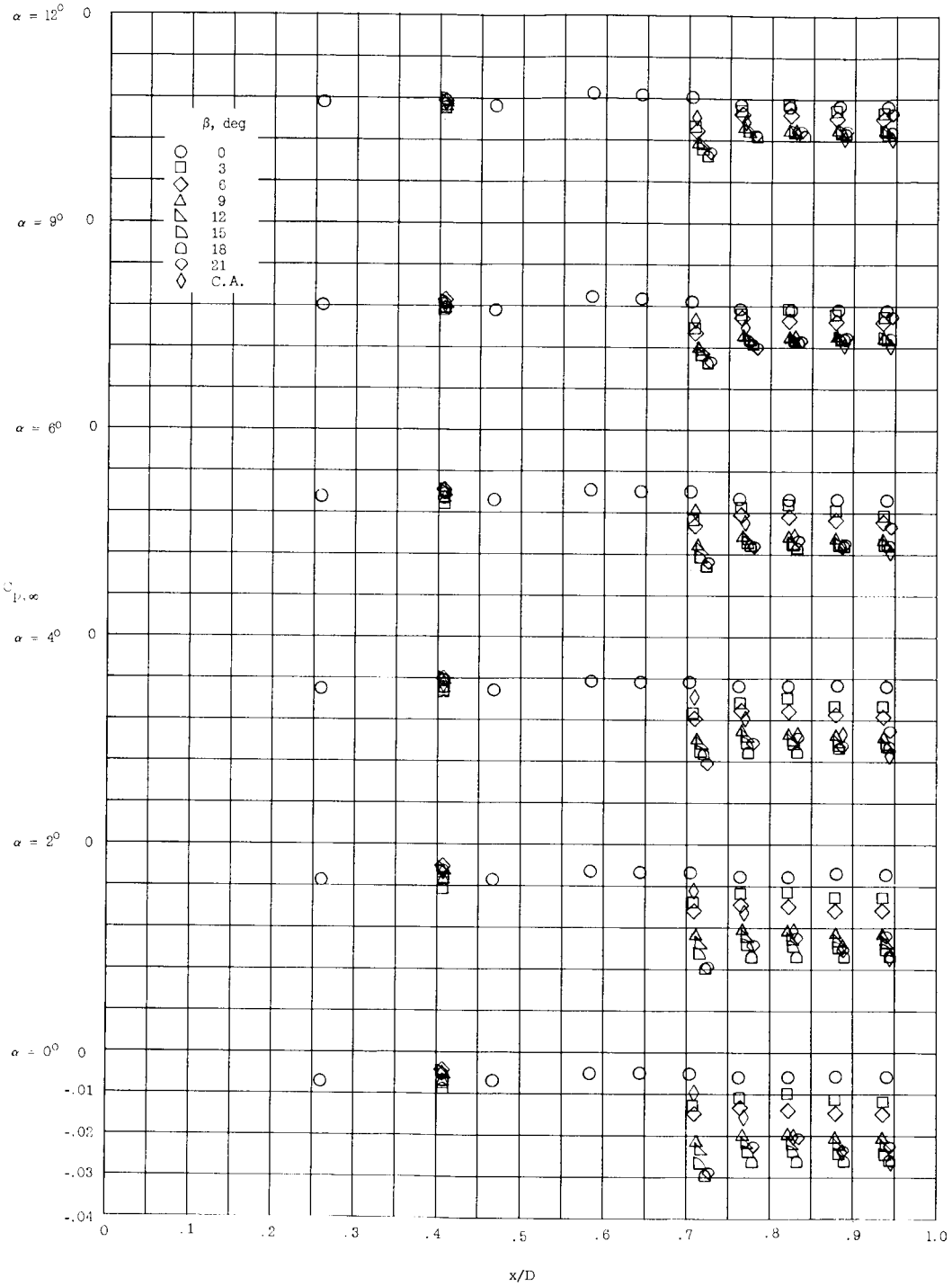

(c) $\phi = 90^\circ$.

Figure 6.- Continued.

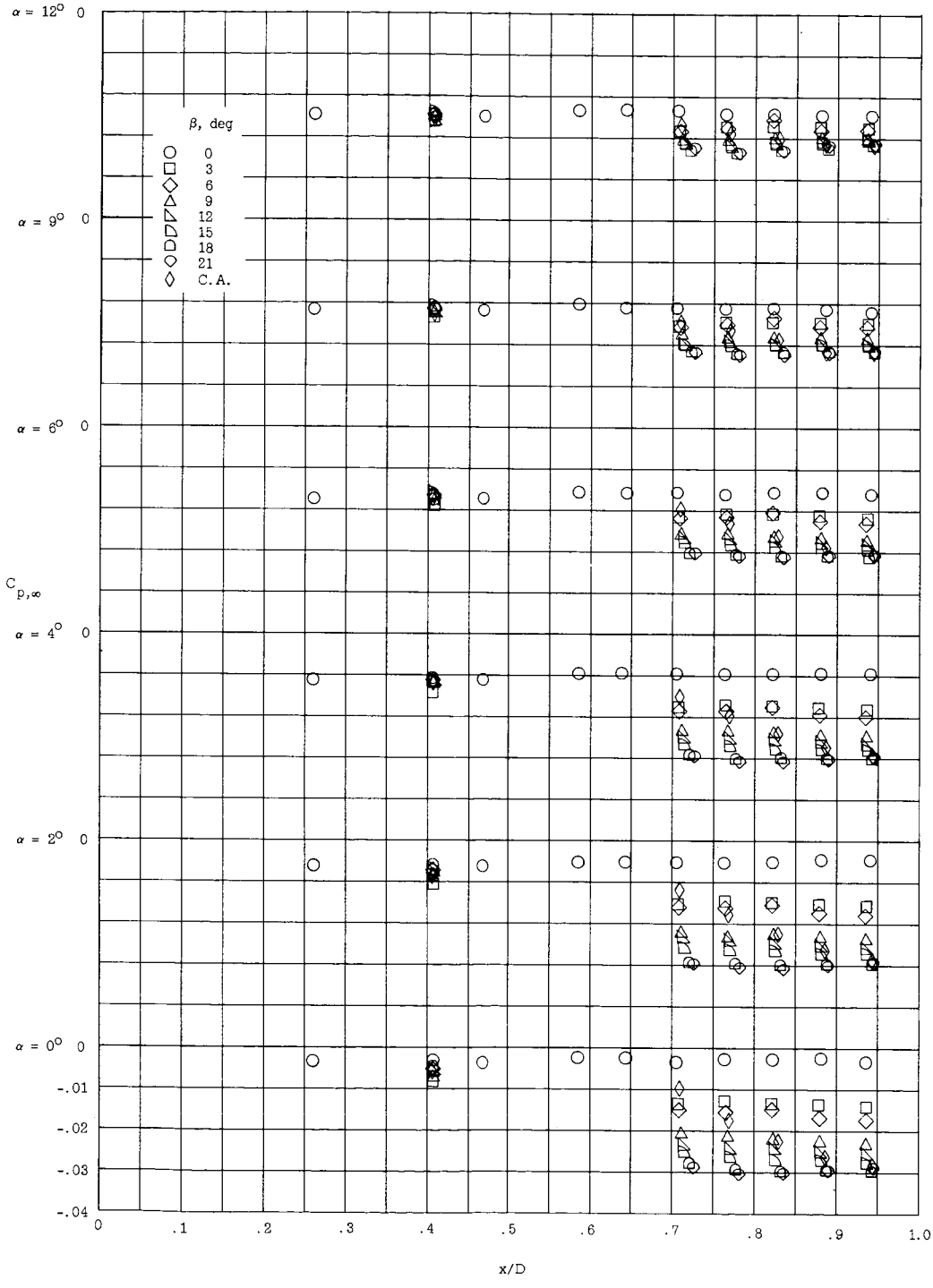

(d) $\phi = 135^{\circ}$.

Figure 6.- Continued.

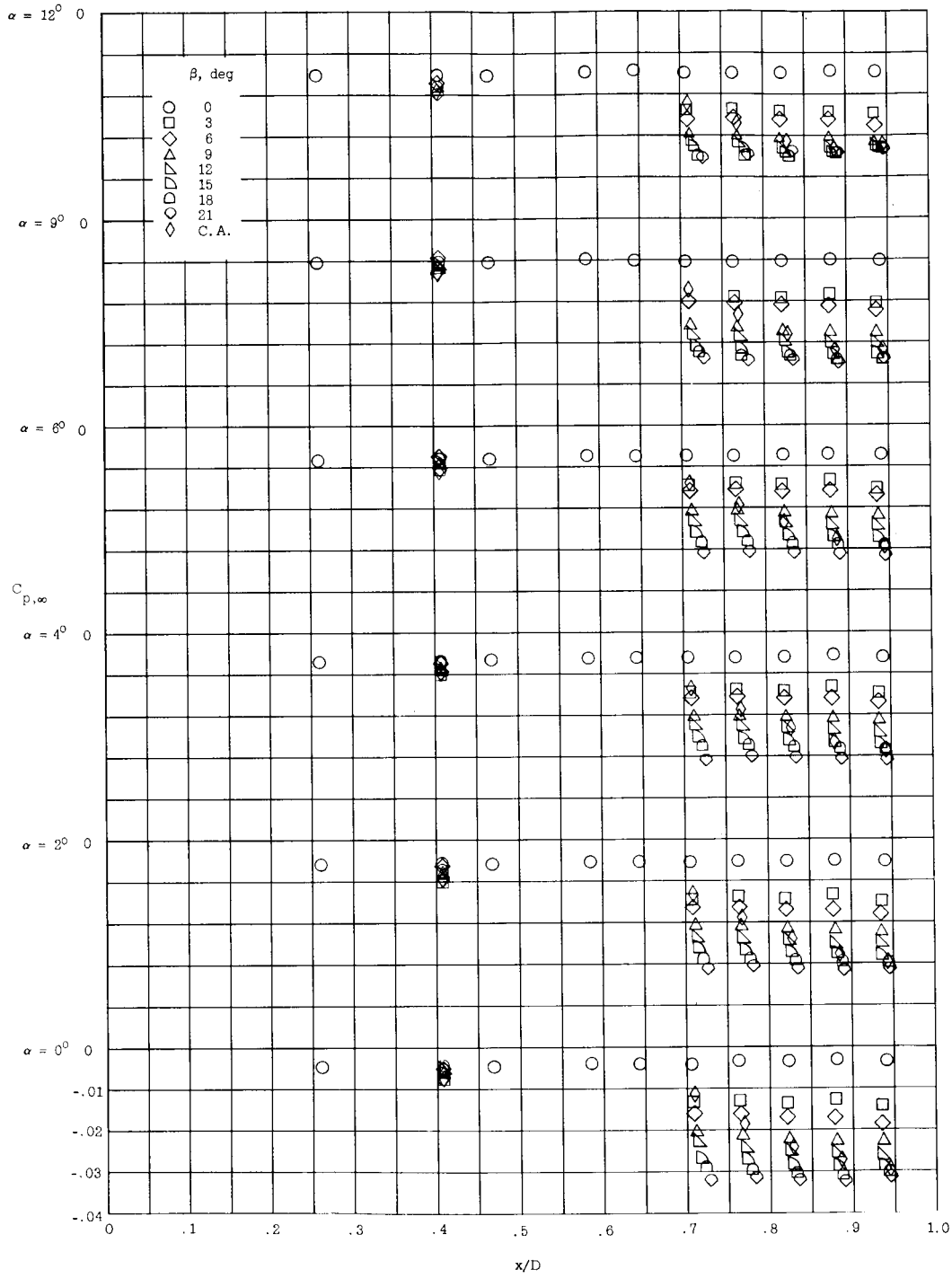

(e) $\phi = 180^{\circ}$.

Figure 6.- Concluded.

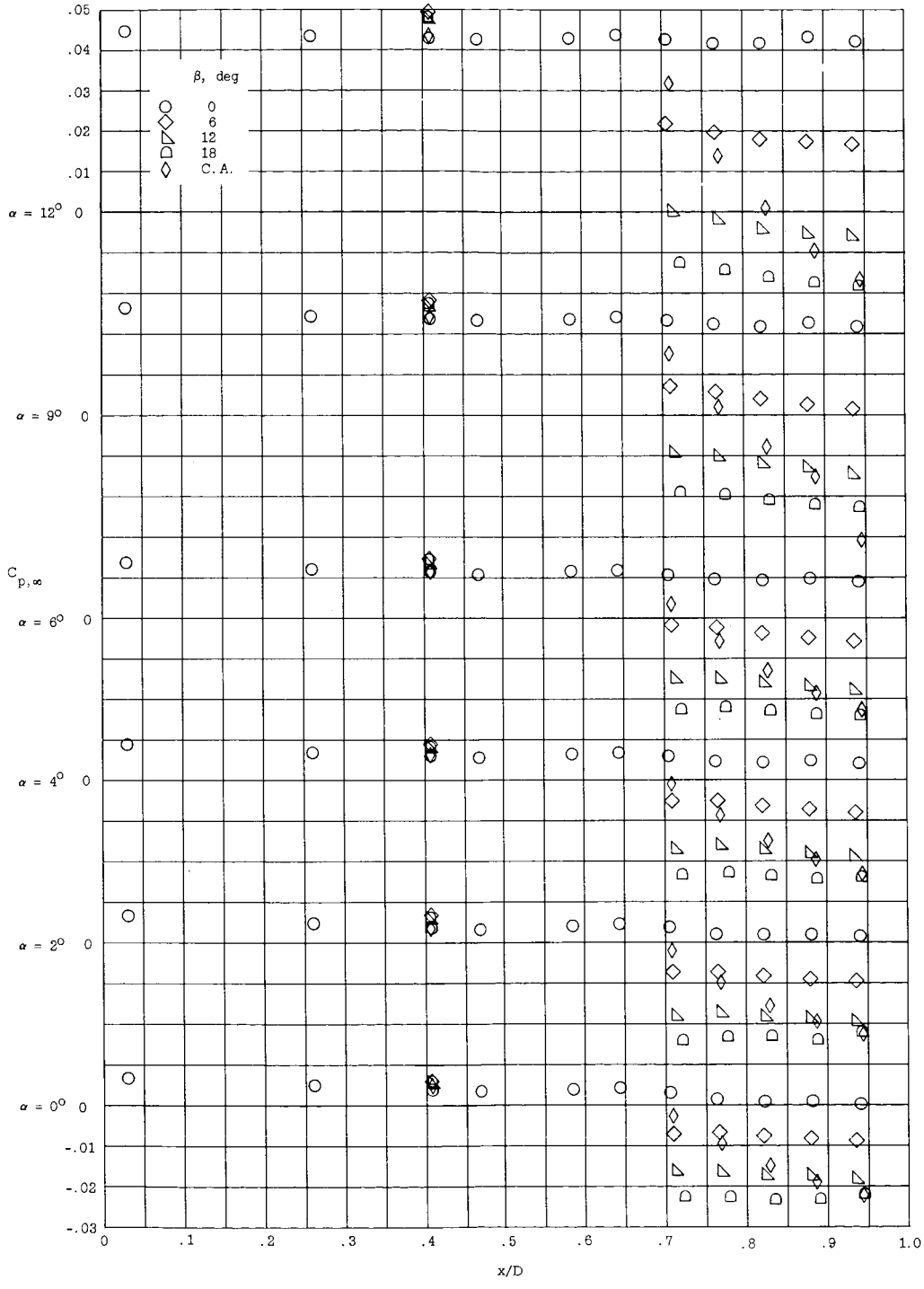

(a) $\phi = 0^{o}$.

Figure 7.- Pressure distribution along the cylinder and afterbody for 45° conical nose section.

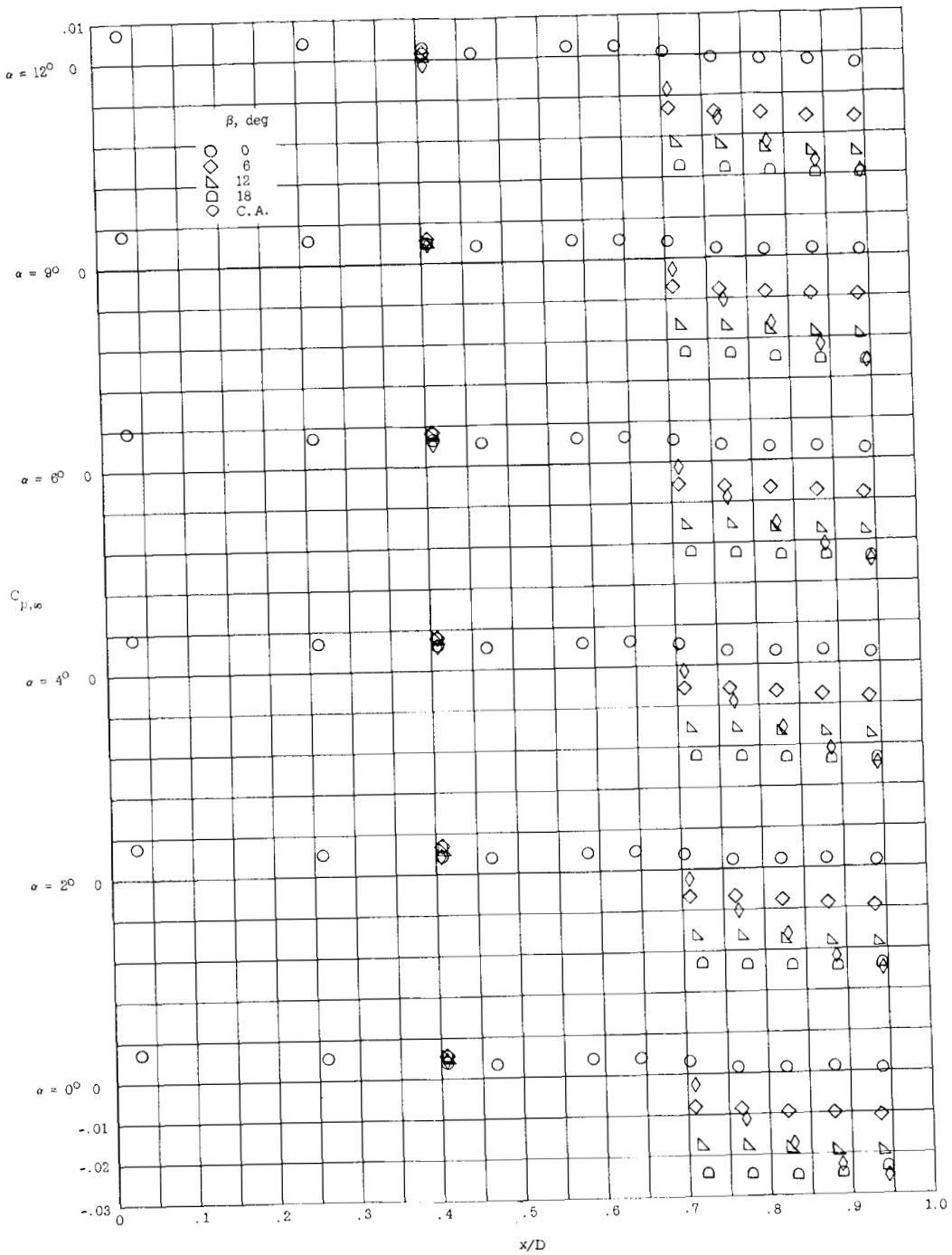

(b) $\phi = 180°$.

Figure 7.- Concluded.

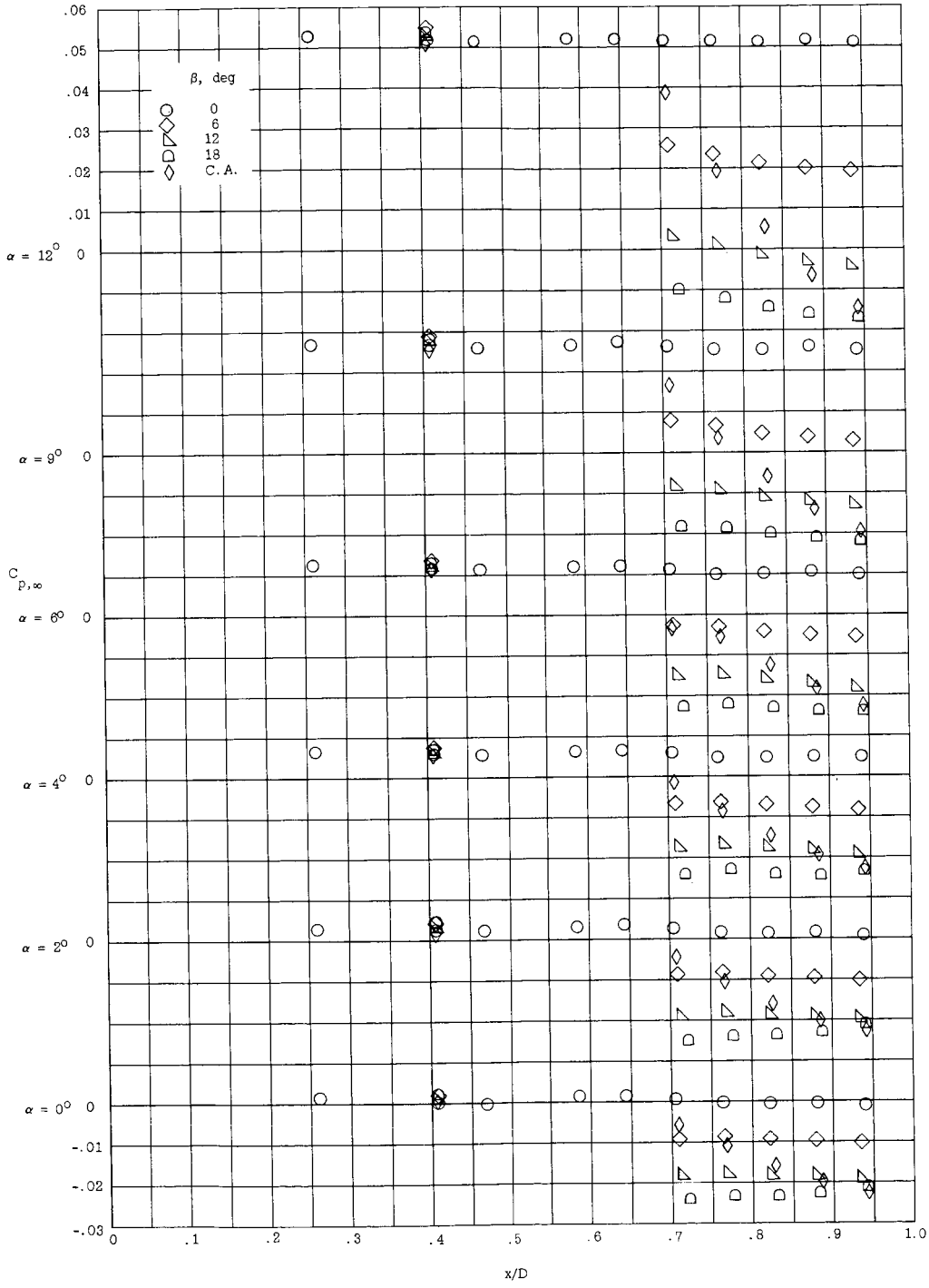

(a) $\phi = 0^{\circ}$.

Figure 8.- Pressure distribution along the cylinder and afterbody for hemispherical nose section.

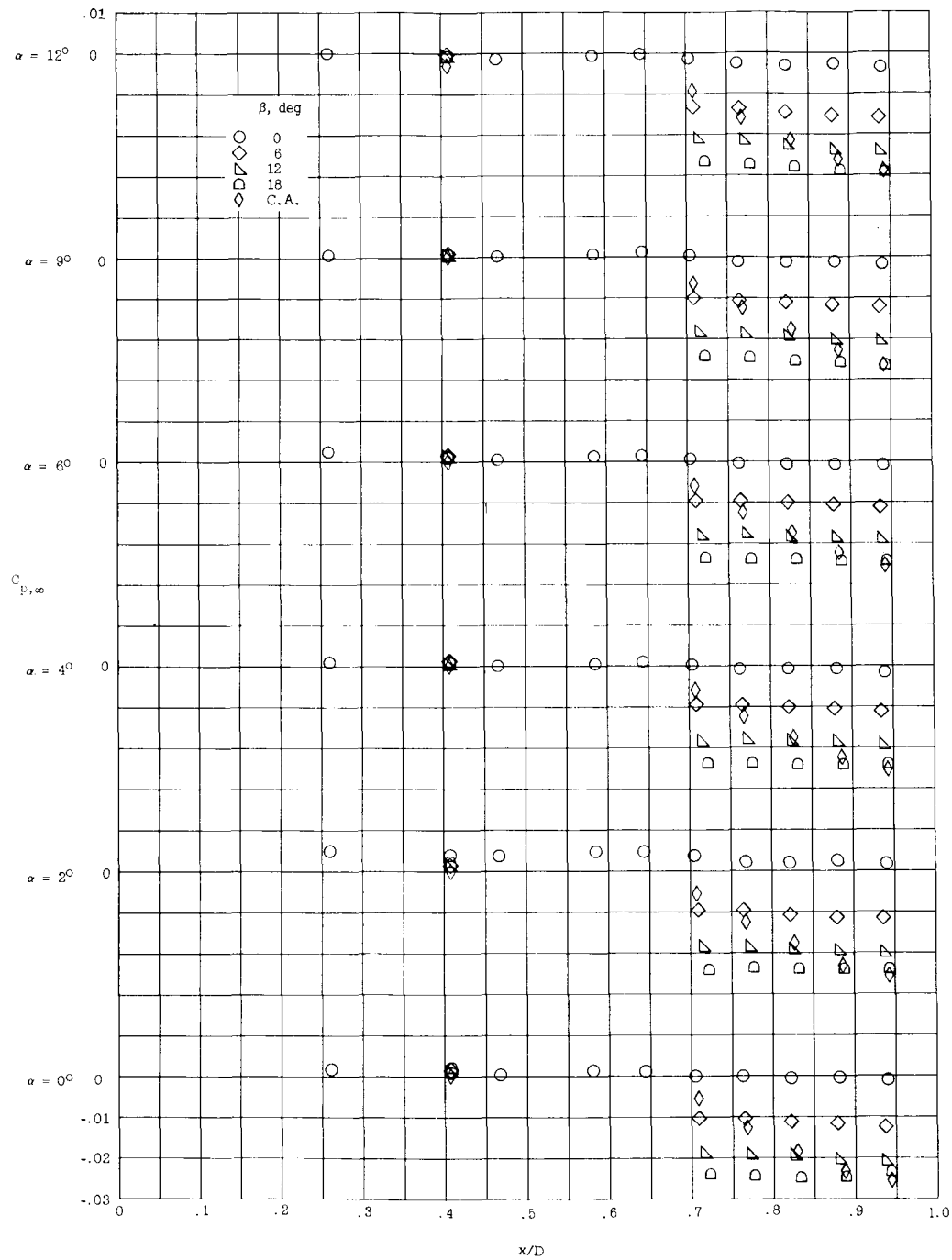

(b) $\phi = 180^{\circ}$.

Figure 8.- Concluded.

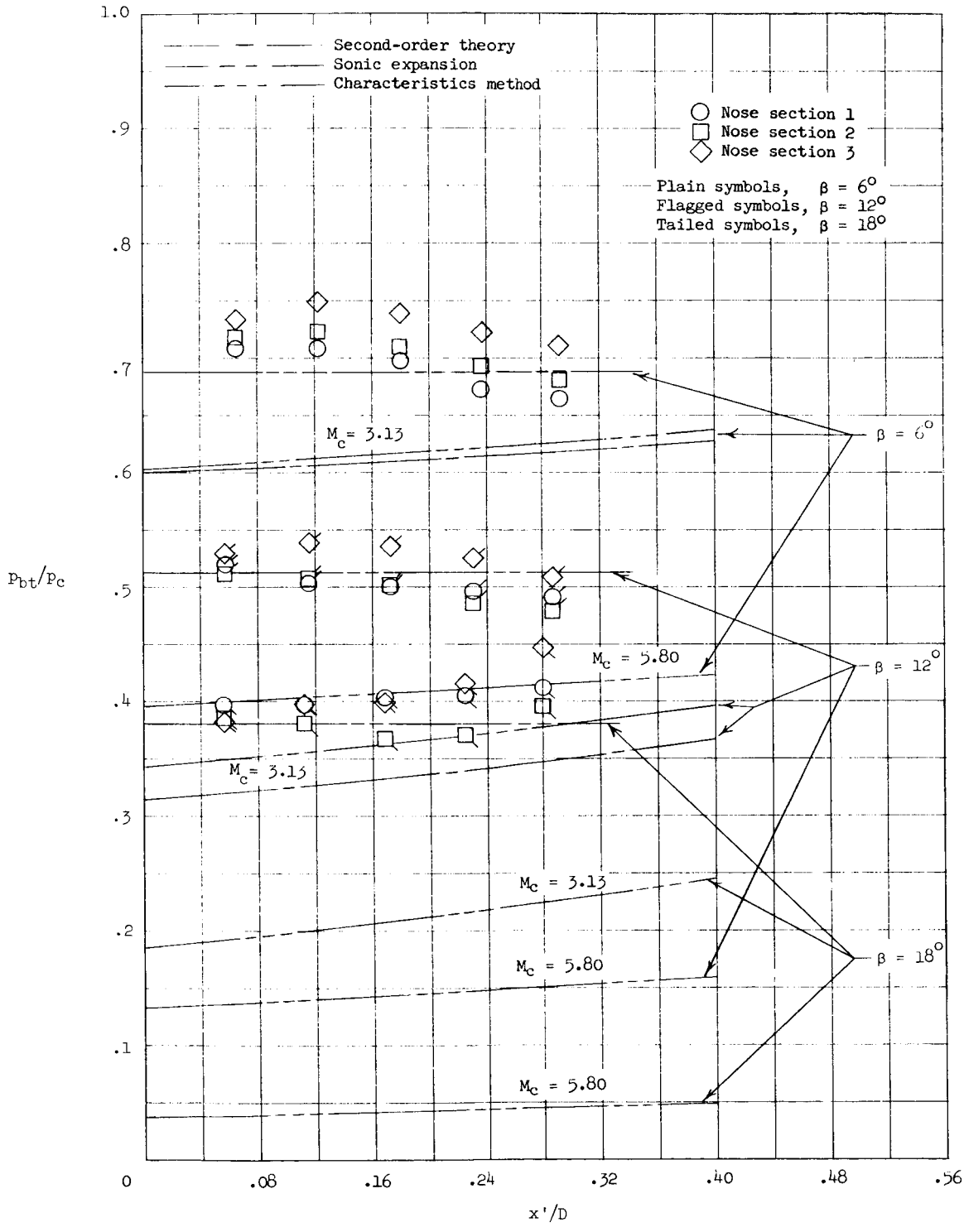

Figure 9.- Comparison of experimental boattail pressures with pressures predicted by several methods. $\alpha = 0^\circ$.

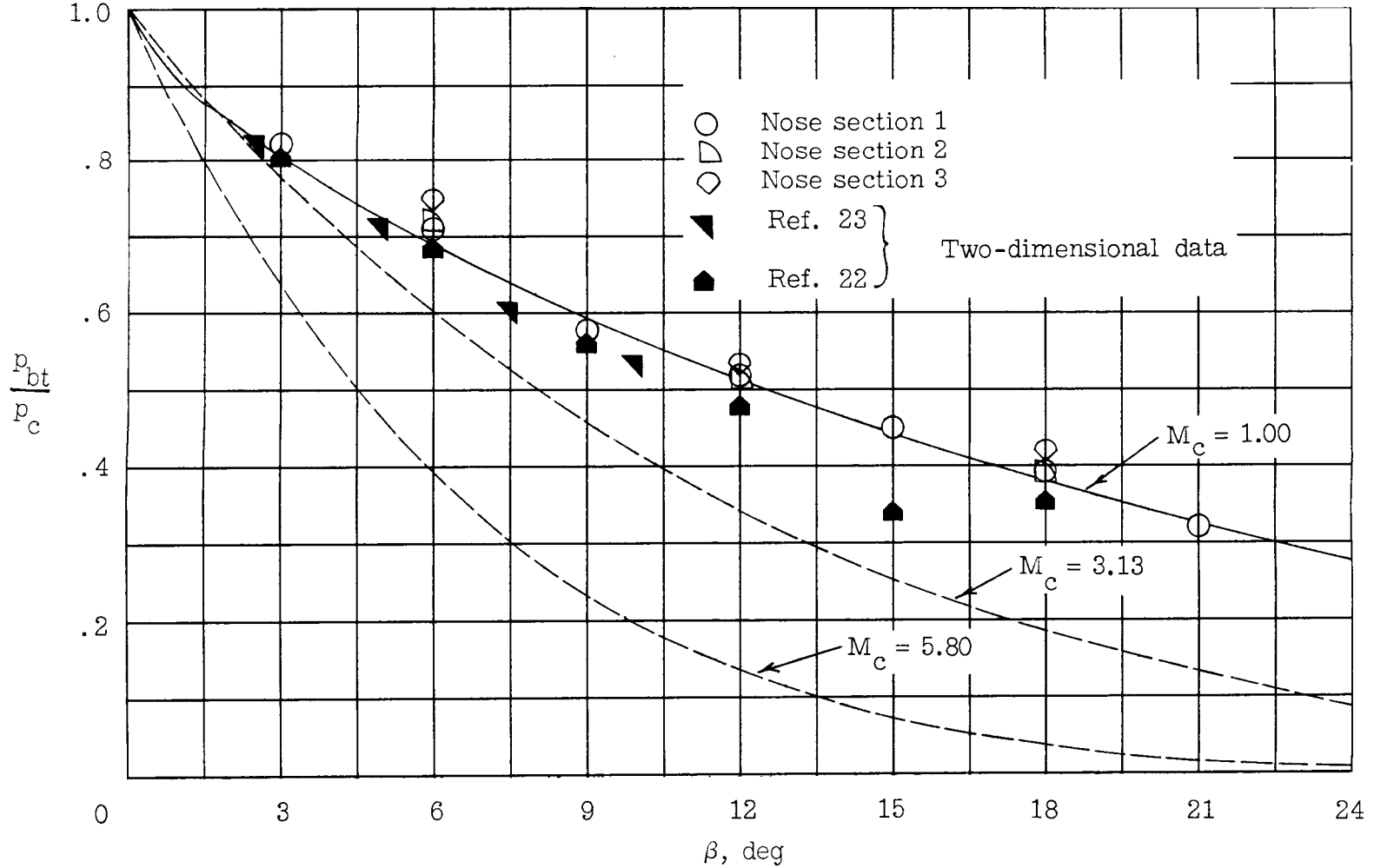

(a) $\alpha = 0^{\circ}$.

Figure 10.- Variation of the average boattail pressure with boattail angle.

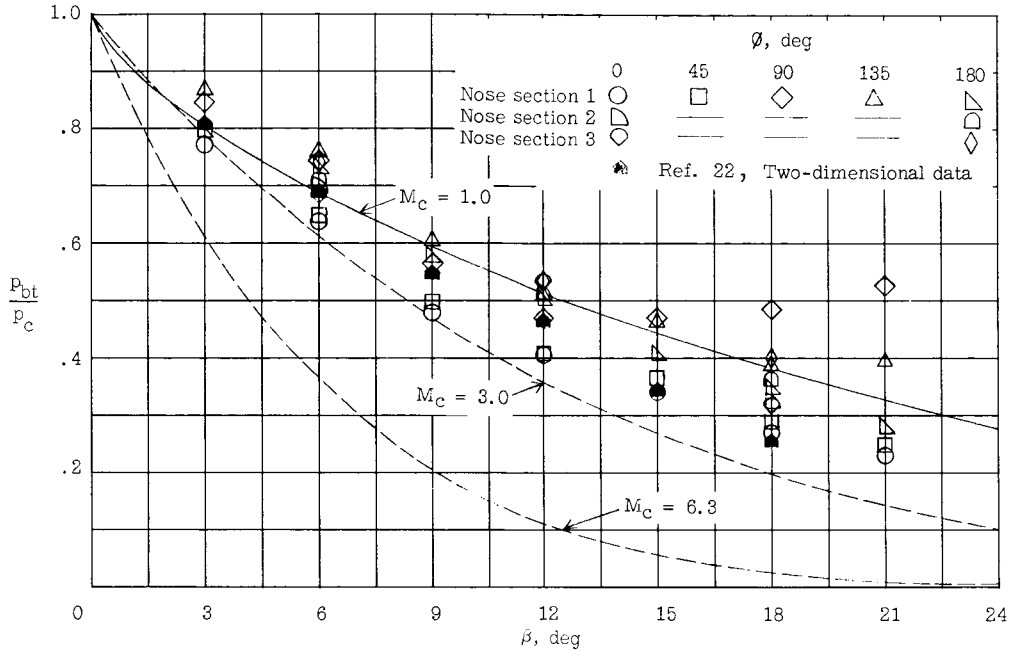

(b) $\alpha = 6^{\circ}$.

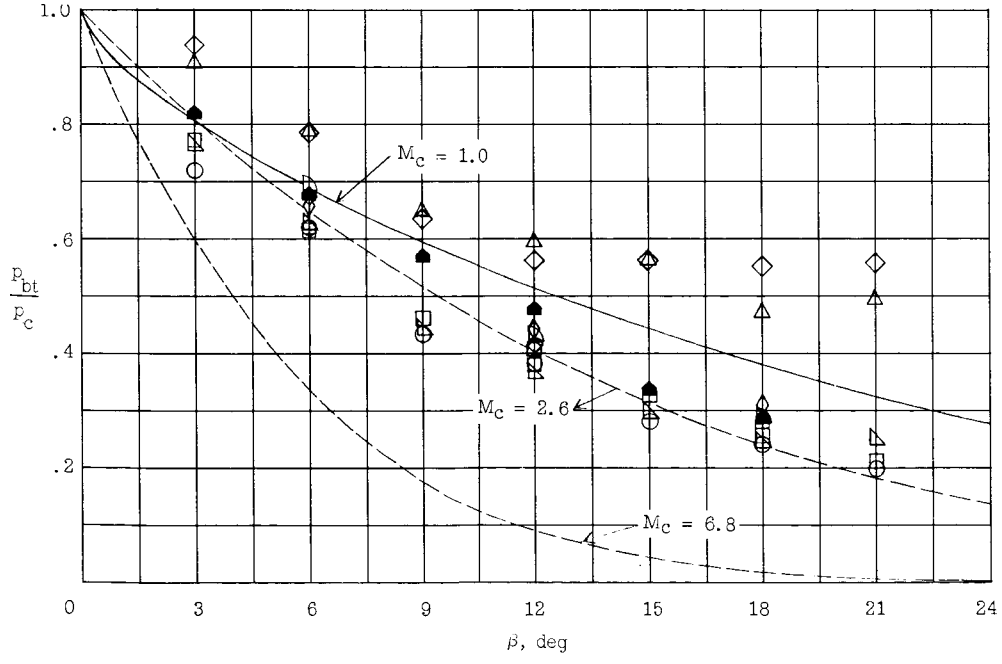

(c) $\alpha = 12^{\circ}$.

Figure 10.- Concluded.

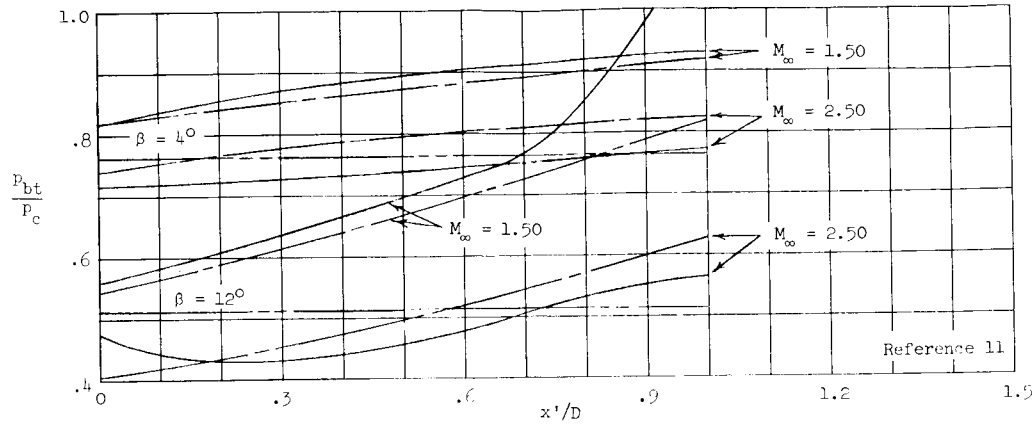

(a) $\beta = 4^\circ$ and 12°.

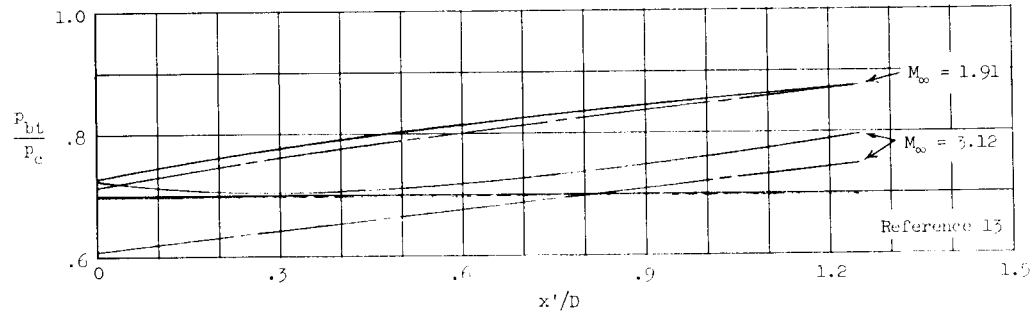

(b) $\beta = 5.63^\circ$.

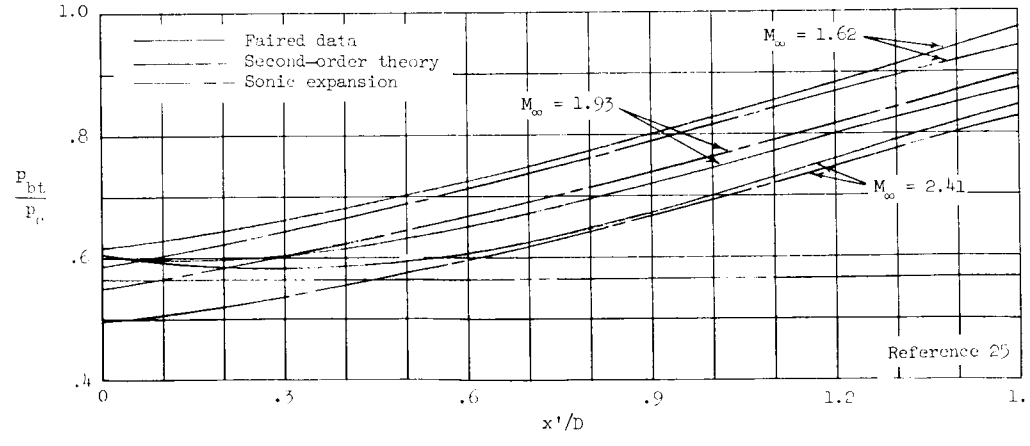

(c) $\beta = 10^\circ$.

Figure 11.- Boattail pressure distributions for various boattail angles and free-stream Mach numbers. $\alpha = 0^\circ$.

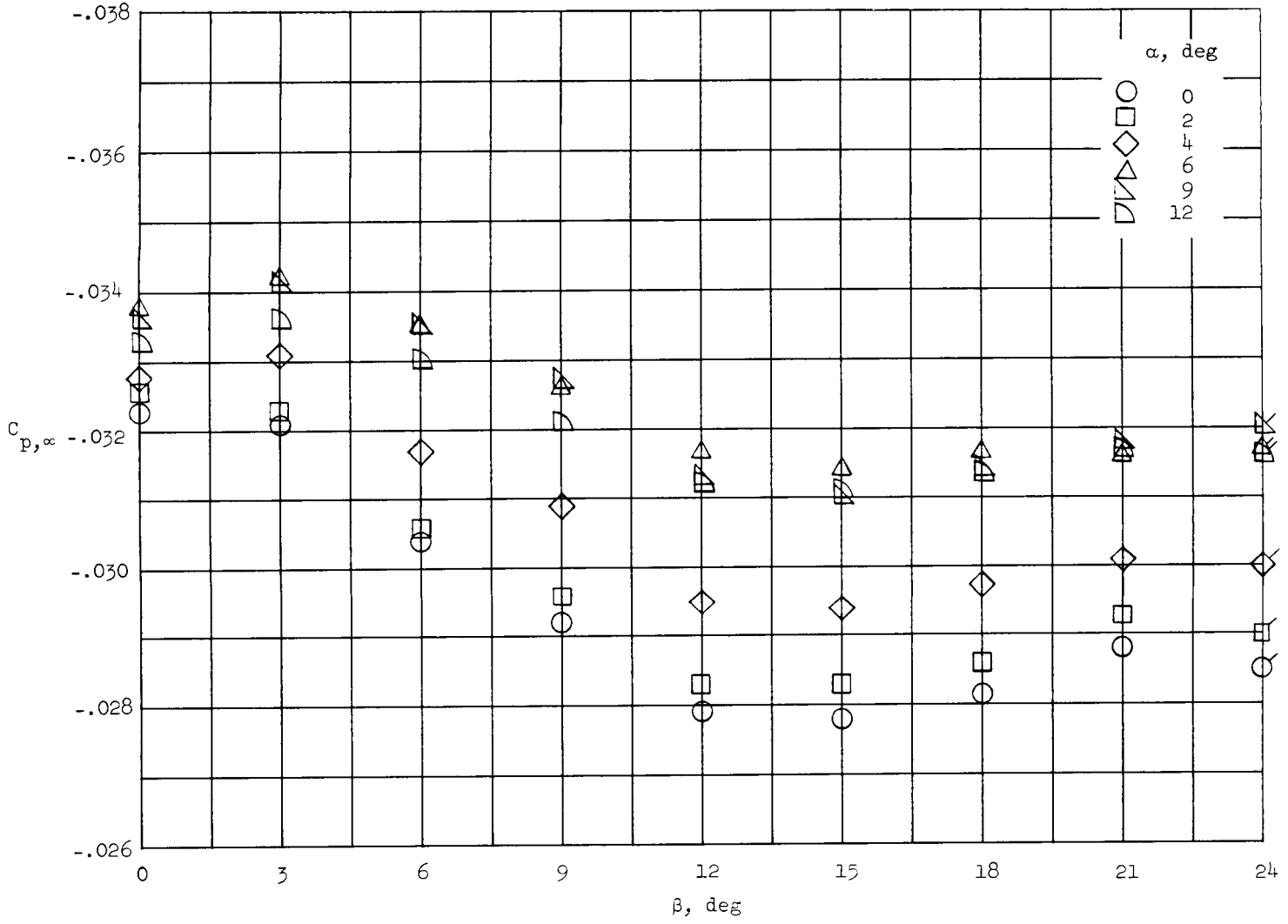

(a) 15° conical nose.

Figure 12.- Effect of boattailing and angle of attack on base pressure coefficient for various nose shapes. $M_\infty = 5.98$. (Flagged symbols denote circular-arc boattail ($\beta = 24^\circ$); see fig. 1(a).)

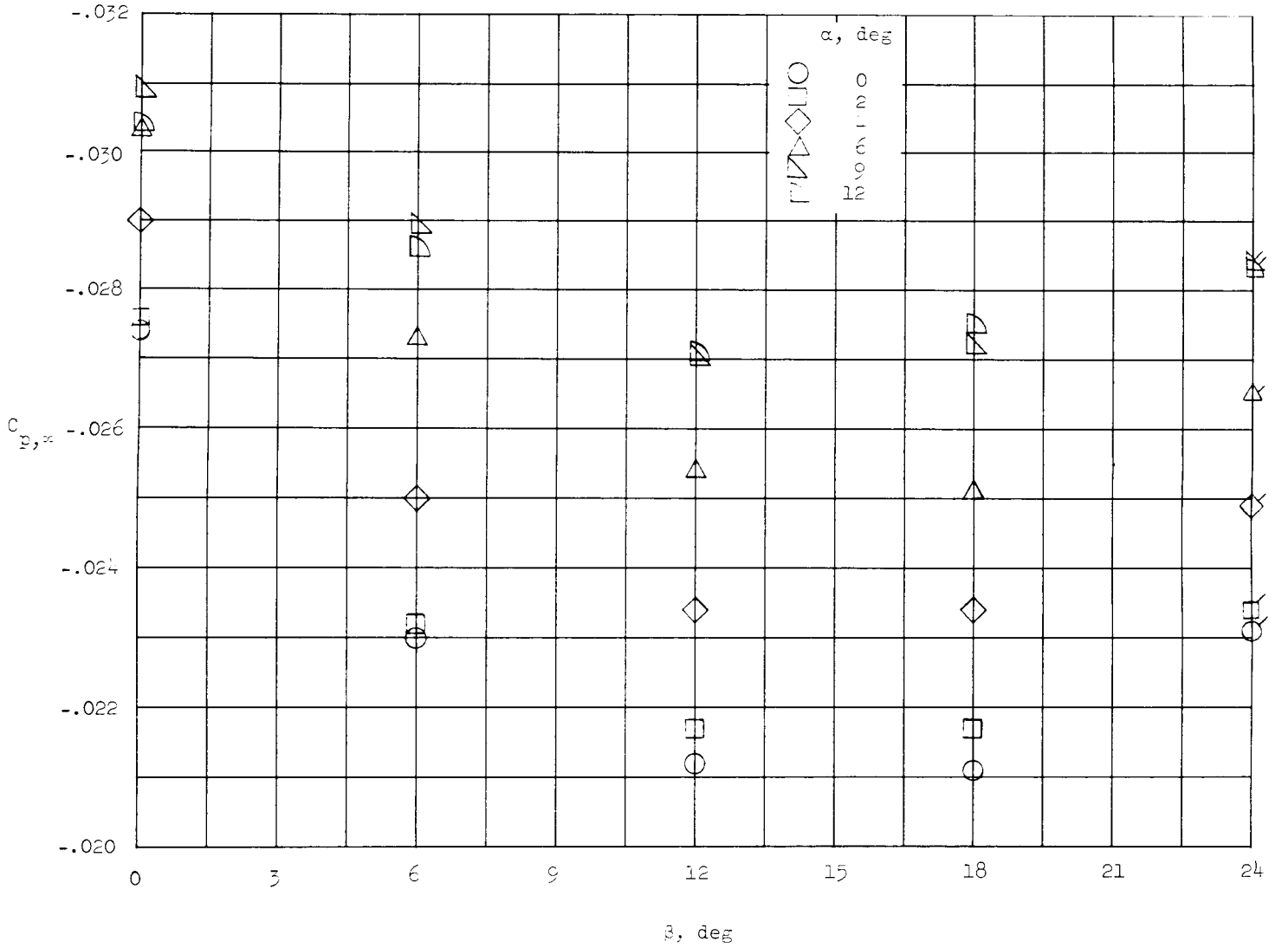

(b) 45° conical nose.

Figure 12.- Continued.

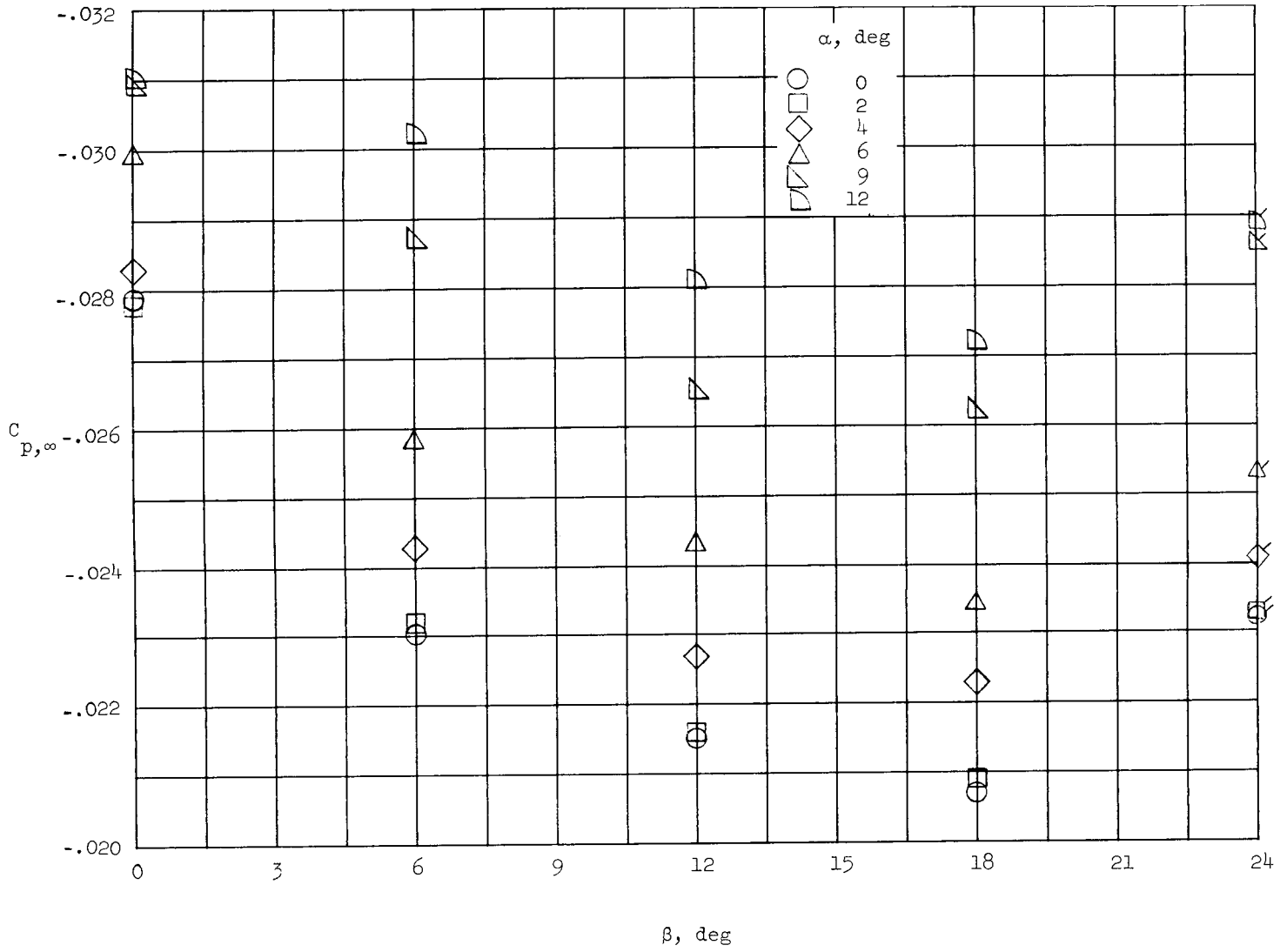

(c) Hemispherical nose.

Figure 12.- Concluded.

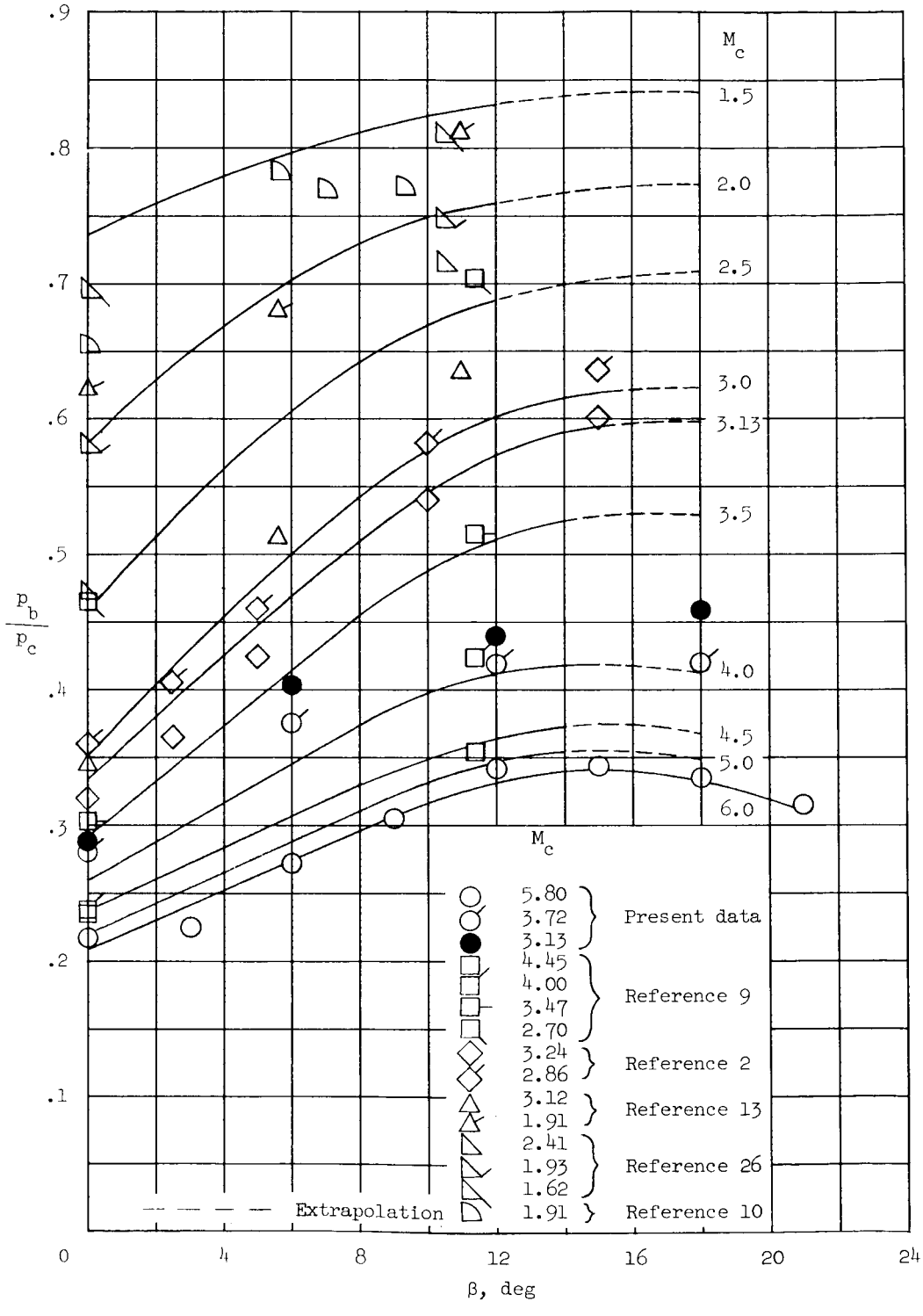

Figure 13.- Compilation of base-pressure data for boattailed bodies of revolution with turbulent boundary layers. $\alpha = 0^{\circ}$.

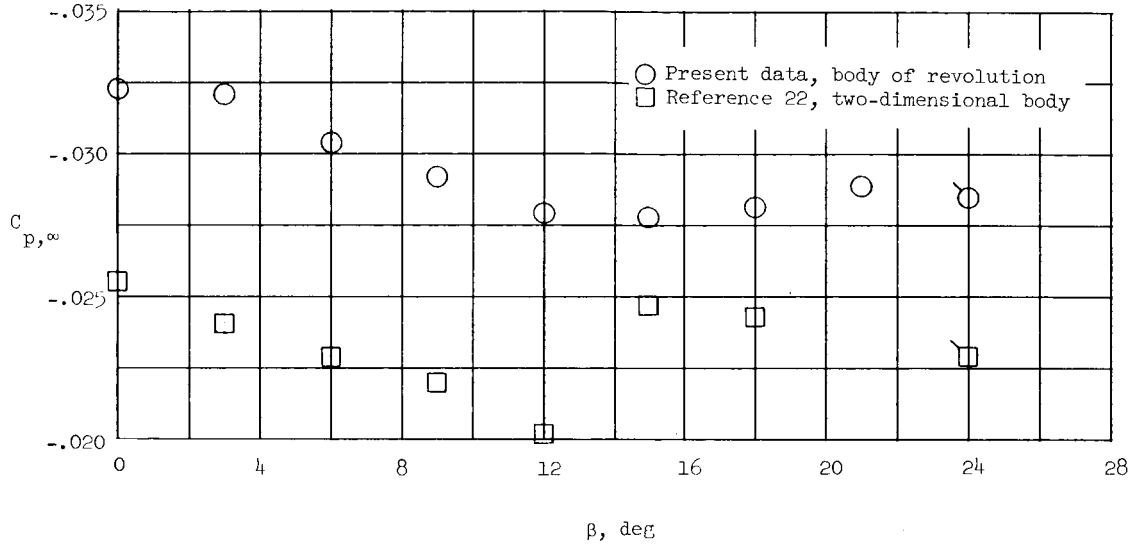

(a) $M_\infty = 5.98$. Flagged symbols denote circular-arc boattail.

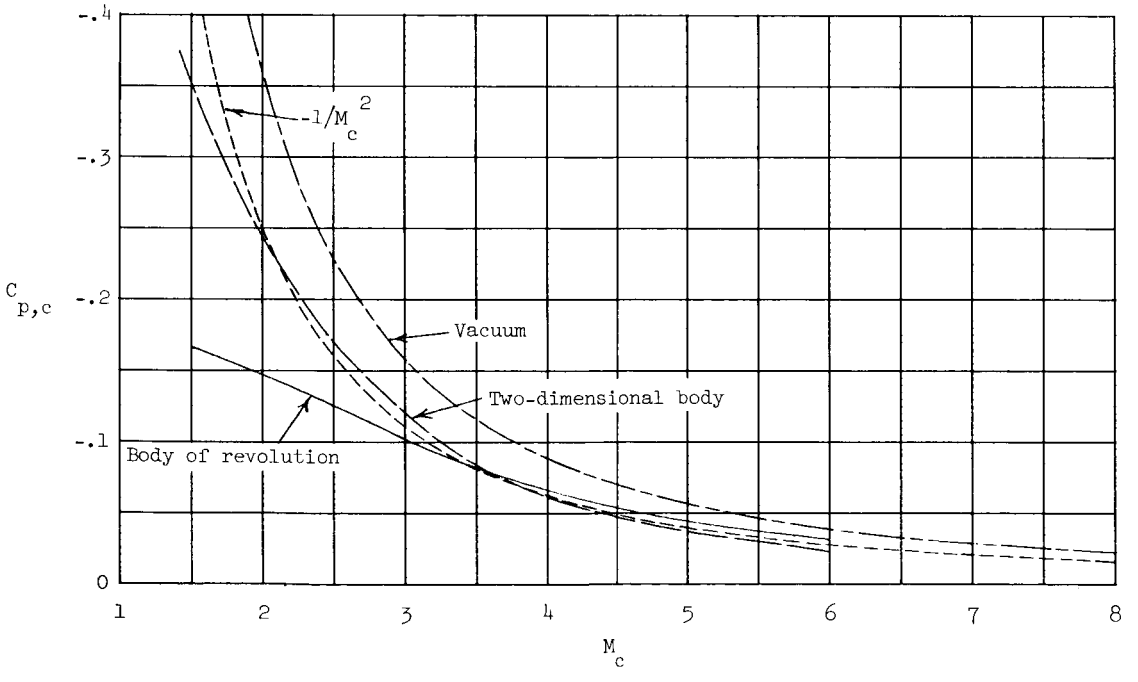

(b) $\beta = 0^\circ$.

Figure 14.- Comparison of base pressure coefficients (based on free-stream and cylinder or flat-plate conditions) for bodies of revolution and two-dimensional bodies. $\alpha = 0^\circ$.

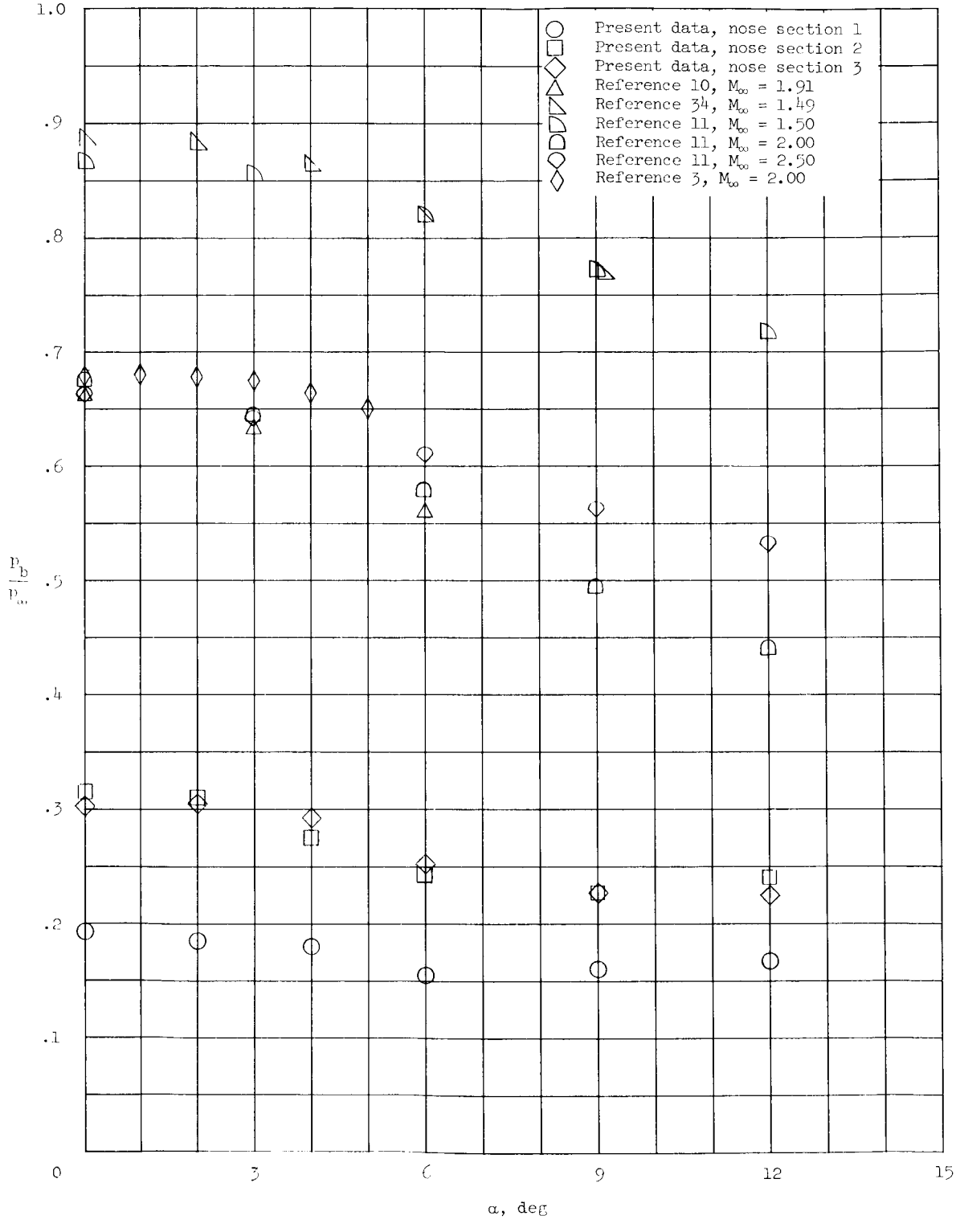

Figure 15.- Effect of angle of attack on base pressure. $\beta = 0^\circ$.

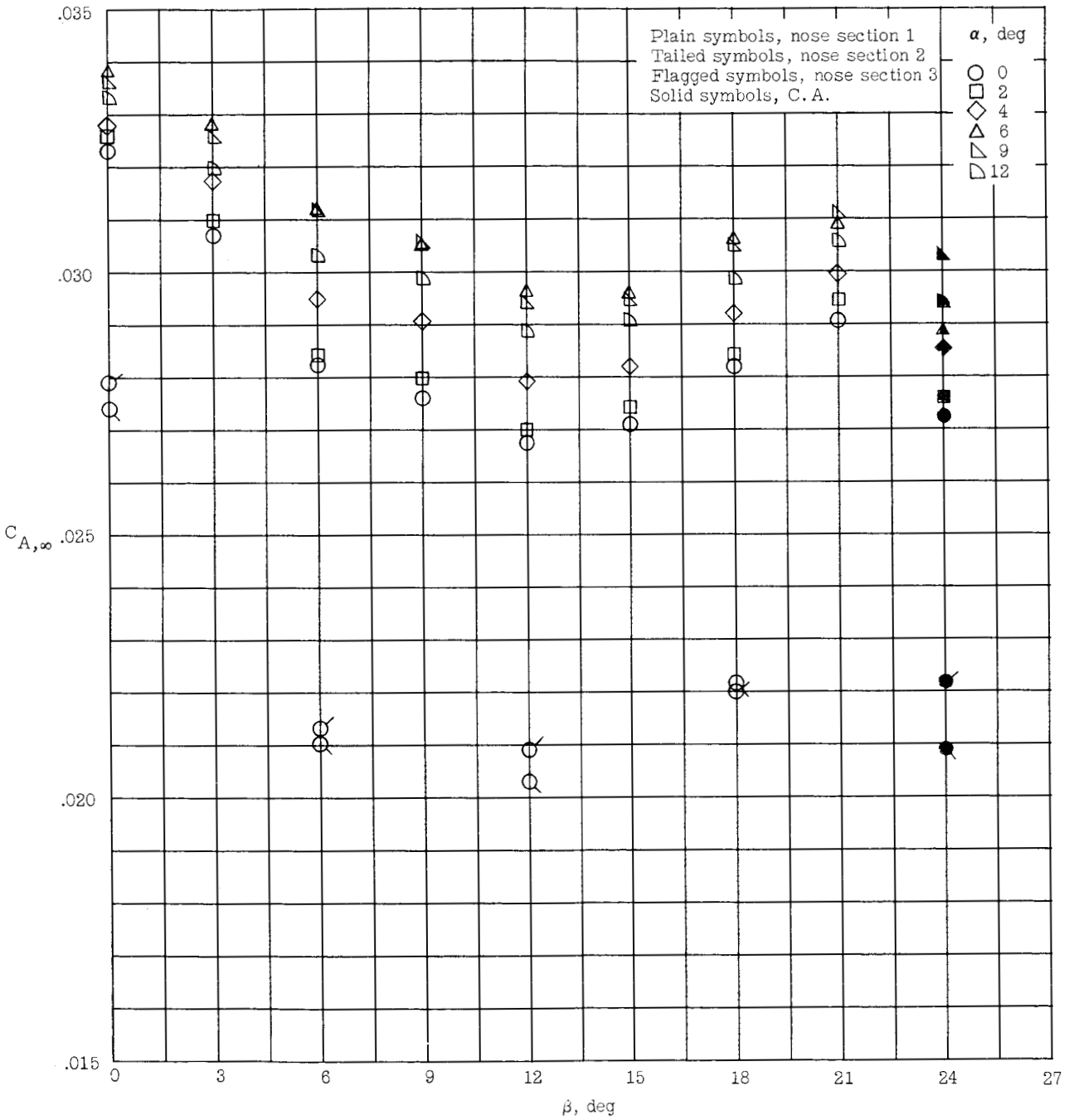

Figure 16.- Variation of afterbody drag with boattail angle.

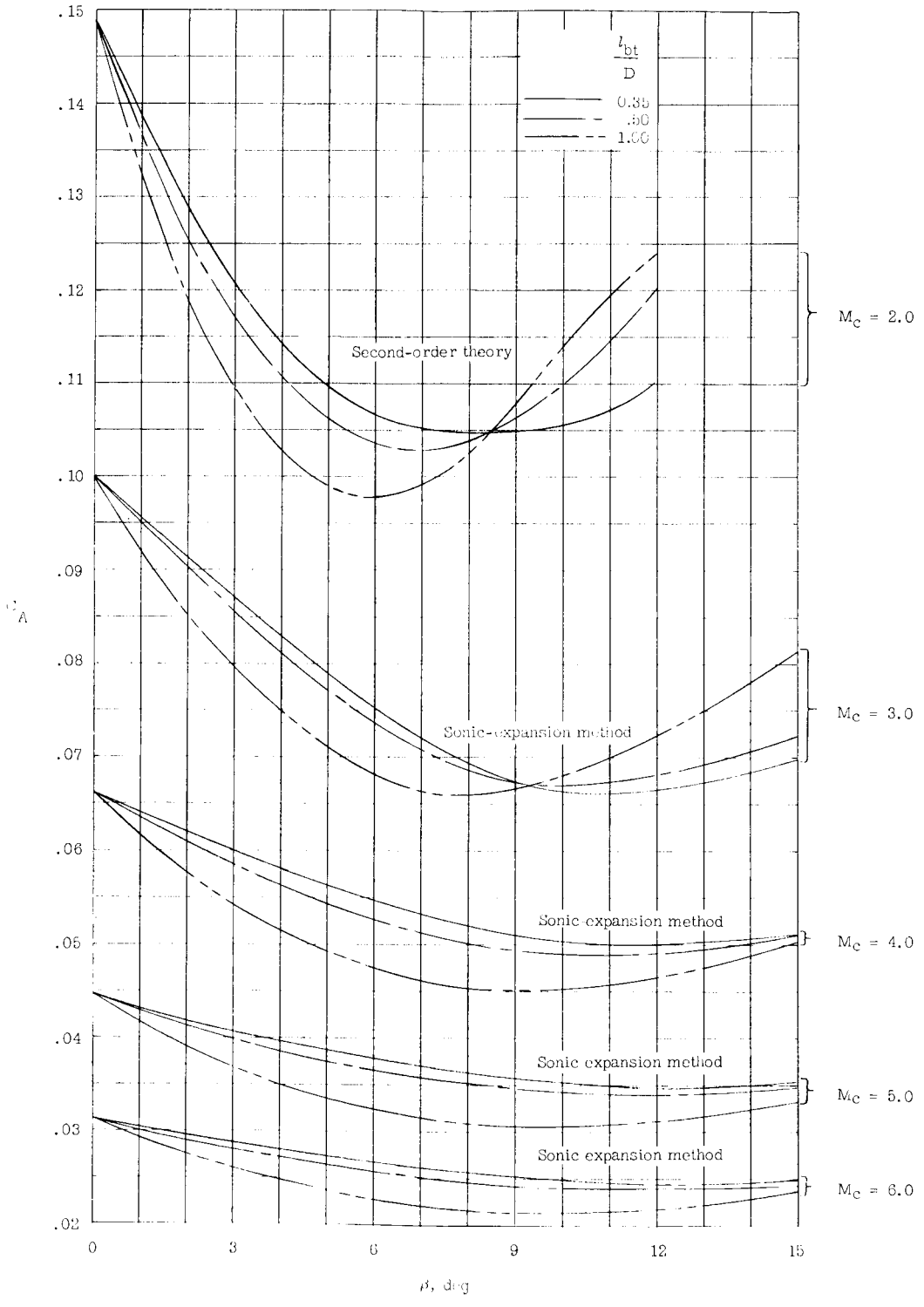

Figure 17.- Variation of afterbody drag with boattail angle for various Mach numbers and boattail lengths. $\alpha = 0^o$.

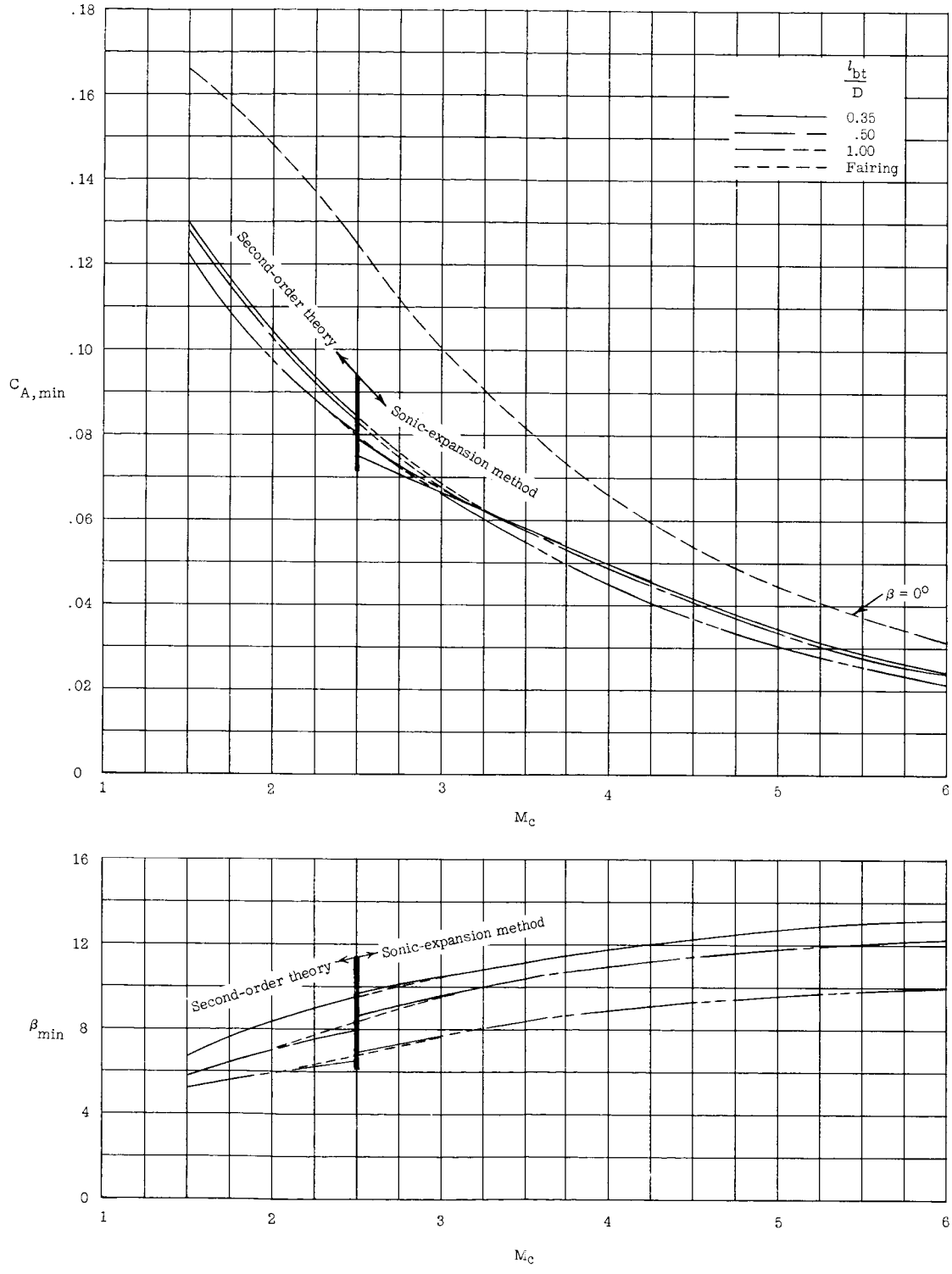

Figure 18.- Minimum afterbody drag and its associated boattail angle as a function of cylinder Mach number and boattail length. $\alpha = 0^{\circ}$.